A Closed Form Reduced Order Electrochemical Model for Lithium-Ion Cells

Journal of The Electrochemical Society, **166** (6) A1197-A1210 (2019)
0013-4651/2019/166(6)/A1197/14/$38.00 © The Electrochemical Society

A Closed Form Reduced Order Electrochemical Model for Lithium-Ion Cells

Ashwini Kumar Sharma,[1,*,a] Suman Basu,[1,b] Krishnan S. Hariharan,[1,z] Shashishekhara P Adiga,[1] Subramanya Mayya Kolake,[1] Taewon Song,[2] and Younghun Sung[2]

[1] *SAIT-India, Samsung R&D Institute India-Bangalore, Bagmane Constellation Business Park, Bangalore 560 037, India*
[2] *Autonomous Material Development Lab, SAIT, Samsung Electronics, Suwon, Korea*

The state of a lithium (Li)-ion cell as a function of measureable quantities like cell voltage and current is not available in closed form without simplifying assumptions like uniform reaction rate, thus limiting the applicability of reduced order electrochemical models for on-board estimation. In the present work, an analytic form for non-uniform reaction rate profile is derived under certain limiting conditions. Using this form and polynomial approximations for the concentration profiles, a direct non-iterative solution scheme is developed for estimation of cell voltage, state of charge (SOC) and other internal variables. The predicted cell voltage is validated against experimental results for commercial cells while the internal variables are verified against the full pseudo 2 dimensional (P2D) model. The results show that, in spite of the order reduction, the model predicts cell voltage as well as the physical processes of the Li-ion cell accurately with less than 1% error for a wide range (0.2C – 5C) of operating conditions. The self-consistent predictive capability along with low computational cost, makes the proposed model an ideal candidate for physics based on-board state estimation.
 [DOI: 10.1149/2.0411906jes]

Manuscript submitted December 28, 2018; revised manuscript received February 27, 2019. Published April 9, 2019.

Application of lithium ion battery has increased manifold in the past decade and is expected to increase further in the coming decades with the advent of electric vehicles.[1,2] A fast and accurate battery management system (BMS) is critical to the success of such large applications of Li-ion battery.[3] Accuracy of a BMS is determined chiefly on the battery state estimation algorithm embedded inside it.[3,4] Most of the BMS uses equivalent circuit based models for state prediction.[4] Although, detailed physics-based electrochemical model P2D[5–7] (pseudo 2-dimensional) offers much greater accuracy and robustness, it is not used due to high computational cost. The P2D model has been applied successfully for estimating the performance at various conditions including variation of operating temperature,[8–14] aging,[15–18] design[19,20] and control.[21,22] The P2D model for Li-ion batteries consider changes in properties in time and space and, thus, consist of coupled nonlinear partial differential equations (PDEs) that govern the conservation of species, energy, and charge in the various layers (current collectors, electrodes, and separator).[5–7,9,11] Such detailed model provides spatially resolved physics inside the cell. However, these are not always preferred for battery packs, onboard battery management system (BMS) algorithms.[23,24] In fact, it is opined that full P2D model based BMS is probably not feasible.[23,24] On the other hand, some recent works aim to make a BMS based on a reformulated P2D[21,22] model framework.

Considering the numerical complexity, many reduced order models have been developed based on the P2D model with simplifying assumptions and/or approximate solutions.[25–44] Assuming uniformity of reaction across the electrode and neglecting the electrolyte resistance, single particle model is developed from P2D model.[25] The model is popular for cycle life modeling due to its simplicity and low computational cost.[25,30] The internal non-uniformity of the cells are neglected in these models. Such assumption is substantiated by estimating the current distribution along the through-plane direction of the electrodes. At moderate charge-discharge rates, the reaction rate is found to be uniform.[30] Cell voltage prediction by this single particle model (SPM) is excellent till 0.7C rate.[25] The cell temperature prediction by SPM matched with detailed model.[30] Similar models have been used for Li-ion battery control.[27–29] Excellent agreement is achieved against full order CFD model.[28] Reduced order models are capable of real-time simulation.[27] Instead of resolving the through-plane dimension, spatial profile with time varying coefficients has been assumed. The profile function is not unique and could be chosen as per the requirement, result etc.[27,29] The coefficients of such profiles can be determined through the boundary conditions.[31] Using volume averaging and uniform reaction rate assumption a reduced order model for Li-ion concentration could be derived.[32] Results of the non-isothermal version of this approach[33] are comparable to full P2D model[14] and experimental data for commercially available NCA (Nickel-Cobalt-Aluminum) batteries at low to medium discharge rates ($\leq$1C). For high rate charge-discharge capability, cubic profile for both electrolyte concentration and potential have been proposed.[34] On the other hand, approximate solutions of Bulter-Volmer equations with quadratic profile approximations in electrolyte phase have also been applied for model high rate operations.[35] Electrochemical parameter evaluation through inversion of reduced order model have been reported recently.[36,37] Single particle model has been applied for optimizing charging profile.[38] BMS for electric vehicle have been developed using such reduced order model.[40] Utilizing principles of control theory and reformulation, electrochemical model based BMS for electric vehicle has also been reported.[44]

It is extremely important to develop an electrochemical model that can accurately predict the cell voltage as well as the internal cell dynamics at moderate computational cost, with no additional mathematical frameworks. In the present work, a reduced order model is developed which retains the robustness and accuracy of the P2D model while computationally economical enough to be implemented onboard. A closed analytical form for the non-uniform reaction rate is developed that naturally evolves into spatial dependence for other internal variables. The proposed model is called non-uniform reduced order model (NUROM) henceforth. The results are validated against results published in literature[45] and also P2D model of commercial FEM based software COMSOL. As multiple processes take place inside the cell (e.g. diffusion in solid phase, diffusion through concentrated solution, reaction at the solid-electrolyte interface etc.), merely matching the cell voltage does not necessarily mean that all the internal processes have been properly modelled. This is especially true for reduced order models, as order reduction assumptions might result in non-physical profiles for individual process models. Therefore, internal variables like reaction rate, electrolyte phase lithium concentration are compared between NUROM and COMSOL to ascertain the quality of the model. An ensuing discussion on the non-monotonic trends for the internal variables and comparison with NUROM showcase the

*Electrochemical Society Member.
[a]Present address: Department of Chemical and Biochemical Engineering, Indian Institute of Technology, Patna 801106, India.
[b]Present address: Energy Systems Department, Mahindra Electric Mobility Limited, Bangalore 560068, India.
[z]E-mail: krishnan.sh@samsung.com

ability of the proposed model to represent the complete physics of Li-ion battery processes.

Full Electrochemical Model

The electrochemical model for lithium ion cells is well established. However, the equations and the boundary conditions are discussed briefly for later reference when the reduced order model is formulated.

Current balance equations.—The solid and electrolyte phase current balance:

$$\frac{\partial}{\partial x}\left(-\sigma_{1k}\frac{\partial \Phi_1}{\partial x}\right) = -J_k \quad \text{where } k = n,\ p \tag{1}$$

$$\frac{\partial}{\partial x}\left(-\kappa_{2k}\frac{\partial \Phi_2}{\partial x} + 2\kappa_{2k}\frac{RT}{F}(1-t_+)\frac{\partial \ln c_2}{\partial x}\right) = J_k \quad \text{where } k = n,\ p,\ s \tag{2}$$

Here, the subscripts, k denote negative electrode, positive electrode, and separator, respectively. Φ_1 is solid phase potential, σ_{1k} is the electrical conductivity of $k = n,\ p$, Φ_2 is the electrolyte phase potential, κ_{2k} is the effective ionic conductivity of $k = n,\ p,\ s$, R is the universal gas constant, T is the temperature, t_+ is the electrolyte transference number, and c_2 is the electrolyte concentration. Note that the ionic conductivity is assumed to be constant and independent of the electrolyte concentration. The volumetric reaction current density, J_k is

$$J_k = \begin{cases} 0 & \text{for separator} \\ a_k F j_k & \text{for electrodes} \end{cases} \tag{3}$$

where a_k is the volumetric surface area and F is the Faraday's constant, The reaction rate, j_k is given by the Butler-Volmer equation for electrode kinetics:

$$j_k = j_{k0}\left[\exp\left(\frac{\alpha_a F \eta}{RT}\right) - \exp\left(-\frac{\alpha_c F \eta}{RT}\right)\right] \tag{4}$$

Here, α_a and α_c are the anodic and cathodic transfer coefficient, η is the over-potential given by, $\eta = \Phi_1 - \Phi_2 - U_k$, U_k denotes the open circuit voltage of $k = n,\ p$ electrode and j_{k0} is the pre-factor as defined in Eq. 5.

$$j_{k0} = k_k\sqrt{(c_{sk\,\max} - c_{sk})\,c_{sk}c_2} \tag{5}$$

where k_k is the surface reaction rate constant, c_{sk} and $c_{sk,max}$ are surface solid phase concentration and its maximum value.

At the current collector / electrode interfaces ($x = 0$ and $x = L = l_n + l_s + l_p$) :

$$-\sigma_{1k}\frac{\partial \Phi_1}{\partial x} = I(t) \tag{6}$$

$$-\kappa_{2k}\frac{\partial \Phi_2}{\partial x} = 0 \tag{7}$$

l_n, l_p and l_s are the thicknesses of negative, positive electrode and separator, respectively and $I(t)$ is the applied current density at any time t.

At the separator / electrode interfaces ($x = l_n$ and $x = l_n + l_s$):

$$-\sigma_{1k}\frac{\partial \Phi_1}{\partial x} = 0 \tag{8}$$

$$-\kappa_{2k}\frac{\partial \Phi_2}{\partial x} + 2\kappa_{2k}\frac{RT}{F}(1-t_+)\frac{\partial \ln c_2}{\partial x} = I(t) \tag{9}$$

To solve for the current balance equations, we need a reference potential (either solid or electrolyte potential) somewhere in the cell. Let us define a zero reference potential at the center of the separator.

$$\Phi_2\left(l_n + \frac{l_s}{2}, t\right) = 0 \tag{10}$$

Eliminating J_k between Eqs. 1–2 and then integrating gives total current balance at any point in electrodes:

$$-\sigma_{1k}\frac{\partial \Phi_1}{\partial x} - \kappa_{2k}\frac{\partial \Phi_2}{\partial x} + 2\kappa_{2k}\frac{RT}{F}(1-t_+)\frac{\partial \ln c_2}{\partial x} = I(t) \tag{11}$$

Similarly, integrating Eq. 2 gives total current balance in the separator:

$$-\kappa_{2s}\frac{\partial \Phi_2}{\partial x} + 2\kappa_{2s}\frac{RT}{F}(1-t_+)\frac{\partial \ln c_2}{\partial x} = I(t) \tag{12}$$

Mass balance in the electrolyte.—Mass balance for the lithium ion in liquid/electrolyte phase.

$$\varepsilon_{2k}\frac{\partial c_2}{\partial t} = \frac{\partial}{\partial x}\left(D_{2k}\frac{\partial c_2}{\partial x}\right) + S_k \text{ where } k = n,\ p,\ s \tag{13}$$

where ε_{2k} is the volume fraction of the electrolyte in electrodes or separator, D_{2k} is the effective electrolyte diffusivity and S_k is the source term given as

$$S_k = \begin{cases} 0 & \text{for separator} \\ a_k(1-t_+)j_k & \text{for electrodes} \end{cases} \tag{14}$$

subject to the following boundary and initial conditions.

At the current collector / electrode interfaces ($x = 0$ and $x = \mathrm{L}$) :

$$-D_{2k}\frac{\partial c_2}{\partial x} = 0 \tag{15}$$

At $t = 0$, the electrolyte concentration is known (c_{20}).

$$c_2(x, 0) = c_{20} \tag{16}$$

Mass balance in the solid phase.—Diffusion of lithium inside the particles is governed by

$$\frac{\partial c_{1k}}{\partial t} = \frac{1}{r^2}\frac{\partial}{\partial r}\left(r^2 D_{1k}\frac{\partial c_{1k}}{\partial r}\right);\ k = n,\ p \tag{17}$$

subject to the following boundary and initial conditions

At the surface of the particle ($r = R_k$):

$$-D_{1k}\frac{\partial c_{1k}}{\partial r} = j_k \tag{18}$$

At the center of the particle ($r = 0$):

$$-D_{1k}\frac{\partial c_{1k}}{\partial r} = 0 \tag{19}$$

At $t = 0$,

$$c_{1k}(r, 0) = c_{1k0} \tag{20}$$

Reduced Order Model Development

Reaction rate profiles.—The reaction rate is the most crucial aspect of the electrochemical model. The choice of spatial profile for this quantity could be based on research experience and mathematical intuition.[27] It is the reaction rate that couples the multiple fields (concentration / current) and also the multiple scales (electrode/electrolyte and the solid phase) in the problem. Hence, to obtain any model order reduction, it is important to have an analytical expression for the reaction rate.

It is possible to get a closed form expression for reaction profile of a simplified Li-ion battery system under certain simplifying assumptions. The steps are described in the Appendix. For this solution, Butler-Volmer equation is linearized (Appendix: Eq. A1) and effect

of local concentration on electrolyte potential is neglected (Appendix: Eq. A3). It can be seen that the ensuing reaction profile is exponential. In order to generalize the application of this profile, we retain the functional form, but the coefficients are determined in the complete solution scheme as described in the subsequent sections. The reaction rate profile for the case of $\sigma_{1n} \gg \kappa_{2n}$[45] is assumed.

$$j_n(x,t) = \frac{I(t)}{a_n F l_n} \exp\left[d_{n1}(t)\left(\frac{x}{l_n} - \frac{1}{d_{n2}(t)}\right)\right] \quad [21]$$

$$j_p(x,t) = -\frac{I(t)}{a_p F l_p} \exp\left[d_{p1}(t)\left(\frac{L-x}{l_p} - \frac{1}{d_{p2}(t)}\right)\right] \quad [22]$$

where $L = l_n + l_s + l_p$ is the sum of the thickness of negative electrode, separator and positive electrode, respectively.

The profile approximations (Eqs. 21–22) are subject to the average reaction rates, at any time in the cell given by the equations below.

$$\langle j_n \rangle(t) = \frac{I(t)}{a_n F l_n} \quad [23]$$

$$\langle j_p \rangle(t) = -\frac{I(t)}{a_p F l_p} \quad [24]$$

Here, $\langle f \rangle$ denotes volume average of a function $f(x,t)$ in the electrode regions that is defined as follows: $\langle f \rangle(t) = \frac{1}{l_k} \int_{x=0}^{l_k} f(x,t)dx$ where $k = n, p$.

The assumed reaction profile for each electrode has two unknown parameters d_{k1} and d_{k2} ($k = n, p$). It is possible to express one parameter in terms of the other through mathematical treatment. Applying the averages for the profile approximation of the negative electrode gives the following:

$$1 = \frac{1}{l_n} \int_{x=0}^{l_n} \exp\left[d_{n1}\left(\frac{x}{l_n} - \frac{1}{d_{n2}}\right)\right] dx \quad [25]$$

$$\Rightarrow 1 = \frac{1}{d_{n1}}\left[\exp\left(d_{n1}\left(1 - \frac{1}{d_{n2}}\right)\right) - \exp\left(-\frac{d_{n1}}{d_{n2}}\right)\right] \quad [26]$$

The above can be rewritten to get

$$d_{n2} = \frac{d_{n1}}{\log\left[\frac{-1+e^{d_{n1}}}{d_{n1}}\right]} \quad [27]$$

Similarly, applying the averages for the profile approximation of the positive electrode gives

$$d_{p2} = \frac{d_{p1}}{\log\left[\frac{-1+e^{d_{p1}}}{d_{p1}}\right]} \quad [28]$$

Solid phase current profiles.—With the exponential reaction rate profile, the negative electrode solid phase current balance becomes

$$\frac{\partial}{\partial x}\left(-\sigma_{1n}\frac{\partial \Phi_1}{\partial x}\right) = -\frac{I(t)}{l_n} \exp\left[d_{n1}\left(\frac{x}{l_n} - \frac{1}{d_{n2}}\right)\right] \quad [29]$$

The above equation is integrated with respect to x to get the solid phase current in negative electrode:

$$-\sigma_{1n}\frac{\partial \Phi_1}{\partial x} = \frac{I(t)}{d_{n1}}\left[\exp\left(d_{n1}\left(1 - \frac{1}{d_{n2}}\right)\right) - \exp\left(d_{n1}\left(\frac{x}{l_n} - \frac{1}{d_{n2}}\right)\right)\right] \quad [30]$$

The boundary condition at separator / negative electrode ($x = l_n$), i.e., zero solid phase current is used to arrive the above. Substituting for d_{n2} from Eq. 27 in Eq. 30, the solid phase current in negative electrode can be rewritten as

$$-\sigma_{1n}\frac{\partial \Phi_1}{\partial x} = I(t)\frac{e^{d_{n1}}}{-1+e^{d_{n1}}}\left[1 - \exp\left(-d_{n1} + \frac{d_{n1}x}{l_n}\right)\right] \quad [31]$$

Note that the above equation satisfies the other boundary condition at the current collector / electrode interface ($x = 0$), i.e., the solid phase current is equal to the total current. Similarly, the solid current balance in the positive electrode, under exponential reaction rate profile approximation becomes

$$\frac{\partial}{\partial x}\left(-\sigma_{1p}\frac{\partial \Phi_1}{\partial x}\right) = \frac{I(t)}{l_p} \exp\left[d_{p1}(t)\left(\frac{L-x}{l_p} - \frac{1}{d_{p2}(t)}\right)\right] \quad [32]$$

The above equation is integrated with respect to x to get the solid current in positive electrode:

$$-\sigma_{1p}\frac{\partial \Phi_1}{\partial x} = \frac{I(t)}{d_{p1}}\left[\exp\left(d_{p1}\left(1 - \frac{1}{d_{p2}}\right)\right) - \exp\left(d_{p1}\left(\frac{L-x}{l_p} - \frac{1}{d_{p2}}\right)\right)\right] \quad [33]$$

Note that we use boundary condition at separator / positive electrode ($x = l_n + l_s$), i.e., zero solid phase current to arrive the above. Substituting for d_{p2} from Eq. 28 in Eq. 33, the solid phase current in positive electrode can be rewritten as

$$-\sigma_{1p}\frac{\partial \Phi_1}{\partial x} = I(t)\frac{e^{d_{p1}}}{-1+e^{d_{p1}}}\left[1 - \exp\left(-d_{p1} + \frac{d_{p1}(L-x)}{l_p}\right)\right] \quad [34]$$

Note that the above equation satisfies the other boundary condition at the current collector / electrode interface ($x = L$), i.e., the solid phase current is equal to the total current.

Electrolyte potential profiles.—*Separator.*—Total current balance equation (Eq. 12) is integrated over the separator domain,[32] and the relevant equations for the electrolyte potentials at the interface are obtained. The potential reference is set to zero at the middle of the cell (Eq. 10). The middle of the cell is referred with subscript '*mid*'. The electrode-separator interfaces are at anode and cathode are referred with subscript '*in*' and '*ip*' respectively.

$$\Phi_2(x,t) = 2\Theta \ln\left[\frac{c_2(x,t)}{c_{2mid}(t)}\right] - \frac{I(t)}{\kappa_{2s}}\left[x - \left(l_n + \frac{l_s}{2}\right)\right] \quad [35]$$

where,

$$\Theta = \frac{RT}{F}(1 - t_+) \quad [35a]$$

Using the above expression, the electrolyte potential at the two electrode-separator interfaces can be shown as below.

$$\Phi_{2in}(t) = \Phi_2(l_n,t) = 2\Theta \ln\left[\frac{c_{2in}(t)}{c_{2mid}(t)}\right] + \frac{I(t)l_s}{2\kappa_{2s}} \quad [36]$$

$$\Phi_{2ip}(t) = \Phi_2(l_n + l_s,t) = 2\Theta \ln\left[\frac{c_{2ip}(t)}{c_{2mid}(t)}\right] - \frac{I(t)l_s}{2\kappa_{2s}} \quad [37]$$

Negative electrode.—Substituting the expression for the solid phase current (Eq. 31) in the total current balance and then integrating once with respect to x gives

$$I(t)\frac{e^{d_{n1}}}{-1+e^{d_{n1}}}\left[x - \frac{l_n}{d_{n1}}\exp\left(-d_{n1} + \frac{d_{n1}x}{l_n}\right)\right] - \kappa_{2n}\Phi_2 + 2\kappa_{2n}\Theta \ln c_2 = I(t)x + g(t) \quad [38]$$

where $g(t)$ is some unknown function. The equation above is evaluated at anode-separator interface ($x = l_n$), as shown below.

$$I(t)\frac{e^{d_{n1}}}{-1+e^{d_{n1}}}\left[l_n - \frac{l_n}{d_{n1}}\right] - \kappa_{2n}\Phi_{2in} + 2\kappa_{2n}\Theta \ln c_{2in} = I(t)l_n + g(t) \quad [39]$$

Eliminating g(t) between Equations 38 and 39 gives

$$\Phi_2(x,t) = \Phi_{2in}(t) + 2\Theta \ln\left(\frac{c_2(x,t)}{c_{2in}(t)}\right) + \frac{I(t)}{\kappa_{2n}}(l_n - x) - \frac{I(t)}{\kappa_{2n}}\frac{e^{d_{n1}}}{-1+e^{d_{n1}}}\left[(l_n - x) - \frac{l_n}{d_{n1}}\left(1 - \exp\left(-d_{n1} + \frac{d_{n1}x}{l_n}\right)\right)\right] \quad [40]$$

For later reference, the electrolyte potential at the current collector/negative electrode interface ($x = 0$) is obtained as

$$\Phi_2(x=0,t) = \Phi_{2\text{in}}(t) + 2\Theta \ln\left(\frac{c_2(0,t)}{c_{2\text{in}}(t)}\right) + \frac{I(t) l_n}{\kappa_{2n}}\left[1 - \frac{(d_{n1}-1)\,e^{d_{n1}}+1}{d_{n1}\left(-1+e^{d_{n1}}\right)}\right] \quad [41]$$

Positive electrode.—A similar procedure (to the above for the negative electrode) is followed to get the electrolyte potential in the positive electrode:

$$\Phi_2(x,t) = \Phi_{2\text{ip}}(t) + 2\Theta \ln\left(\frac{c_2(x,t)}{c_{2\text{ip}}(t)}\right) + \frac{I(t)}{\kappa_{2p}}(l_n + l_s - x) + \frac{I(t)}{\kappa_{2p}}\frac{e^{d_{p1}}}{-1+e^{d_{p1}}}\left[(x-l_n-l_s)+\frac{l_p}{d_{p1}}\left(-1+\exp\left(-\frac{d_{p1}(x-l_n-l_s)}{l_p}\right)\right)\right] \quad [42]$$

For later reference, the electrolyte potential at the current collector/positive electrode interface ($x = L$) is obtained as

$$\Phi_2(x=L,t) = \Phi_{2\text{ip}}(t) + 2\Theta \ln\left(\frac{c_2(L,t)}{c_{2\text{ip}}(t)}\right) - \frac{I(t) l_p}{\kappa_{2p}}\left[1 - \frac{(d_{p1}-1)e^{d_{p1}}+1}{d_{p1}\left(-1+e^{d_{p1}}\right)}\right] \quad [43]$$

Estimation of coefficients of exponential argument in rate profile approximations.—There are two unknown coefficients (d_{k1} *and* d_{k2}) in exponential argument in the reaction rate profile approximations for each electrode. Applying the average reaction rates, we have already found equations expressing d_{k2} in terms of d_{k1} (Eqs. 27–28). In this section, a procedure to determine d_{k1} is detailed. The Bulter–Volmer equation (Eq. 4) for the electrode kinetics (assuming $\alpha_a = \alpha_c$) can be written as:

$$j_k = j_{k0}\sinh\left[\frac{F}{2RT}\left(\Phi_1 - \Phi_2 - U_k\right)\right] \quad [44]$$

or

$$\sinh^{-1}\left(\frac{j_k}{j_{k0}}\right) = \sinh^{-1}(z) = \frac{F}{2RT}\left(\Phi_1 - \Phi_2 - U_k\right); z = \frac{j_k}{j_{k0}} \quad [45]$$

As $\sinh^{-1}(z) = \log\lfloor z + \sqrt{1+z^2}\rfloor = \log(z) + \log\lfloor 1 + \sqrt{1+z^{-2}}\rfloor$, the above equation becomes:

$$\log(z) + \log\left[1+\sqrt{1+z^{-2}}\right] = \frac{F}{2RT}\left(\Phi_1 - \Phi_2 - U_k\right) \quad [46]$$

Differentiating both sides of the above equation gives

$$\frac{1}{z}\frac{\partial z}{\partial x}\left[1 \pm \frac{1}{\left(1+z^{-2}+\sqrt{1+z^{-2}}\right)z^2}\right] = \frac{F}{2RT}\left(\frac{\partial \Phi_1}{\partial x} - \frac{\partial \Phi_2}{\partial x} - \frac{\partial U_k}{\partial x}\right) \quad [47]$$

Using expansion of $\sqrt{1+z^{-2}}$ and simplifying,

$$\frac{1}{z}\frac{\partial z}{\partial x}\left[1 \pm \frac{1}{\left(\frac{3}{2}+2z^2\right)}\right] = \frac{F}{2RT}\left(\frac{\partial \Phi_1}{\partial x} - \frac{\partial \Phi_2}{\partial x} - \frac{\partial U_k}{\partial x}\right) \quad [48]$$

$$\text{or} \quad \left(\frac{1}{j_k}\frac{\partial j_k}{\partial x} - \frac{1}{j_{k0}}\frac{\partial j_{k0}}{\partial x}\right)\left[1 \pm \frac{1}{\left(\frac{3}{2}+2\left(\frac{j_k}{j_{k0}}\right)^2\right)}\right] = \frac{F}{2RT}\left(\frac{\partial \Phi_1}{\partial x} - \frac{\partial \Phi_2}{\partial x} - \frac{\partial U_k}{\partial x}\right) \quad [49]$$

From total current balance, we have

$$-\frac{\partial \Phi_2}{\partial x} = \frac{I(t)}{\kappa_{2k}} + \frac{\sigma_{1k}}{\kappa_{2k}}\frac{\partial \Phi_1}{\partial x} - 2\frac{RT}{F}(1-t_+)\frac{\partial \ln c_2}{\partial x} \quad [50]$$

Substituting the above in Eq. 49 gives:

$$\left(\frac{1}{j_k}\frac{\partial j_k}{\partial x} - \frac{1}{j_{k0}}\frac{\partial j_{k0}}{\partial x}\right)\left[1 \pm \frac{1}{\left(\frac{3}{2}+2\left(\frac{j_k}{j_{k0}}\right)^2\right)}\right] = \frac{F}{2RT}\left[\frac{I(t)}{\kappa_{2k}} + \left(1+\frac{\sigma_{1k}}{\kappa_{2k}}\right)\frac{\partial \Phi_1}{\partial x} - 2\Theta\frac{\partial \ln c_2}{\partial x} - \frac{\partial U_k}{\partial x}\right] \quad [51]$$

Negative electrode.—Substituting for j_n from Eq. 21 and $\partial\Phi_1/\partial x$ from Eq. 31 from solid current balance in Eq. 51 results in

$$\left(\frac{d_{n1}}{l_n} - \frac{1}{j_{n0}}\frac{\partial j_{n0}}{\partial x}\right)\left[1 \pm \frac{1}{\left(\frac{3}{2}+2\left(\frac{j_n}{j_{n0}}\right)^2\right)}\right] = \pm\frac{F}{2RT}\left[\begin{array}{l}\frac{I(t)}{\kappa_{2n}} - \left(1+\frac{\sigma_{1n}}{\kappa_{2n}}\right)\frac{I(t)}{\sigma_{1n}}\frac{e^{d_{n1}}}{-1+e^{d_{n1}}}\left[1-\exp\left(-d_{n1}+\frac{d_{n1}x}{l_n}\right)\right] \\ -2\Theta\frac{\partial \ln c_2}{\partial x} - \frac{\partial U_n}{\partial x}\end{array}\right] \quad [52]$$

where the positive and negative sign on the RHS are for discharge and charge, respectively. Volume averaging both sides of the above equation

$$\left[\frac{d_{n1}}{l_n} - \left\langle\frac{\partial \ln j_{n0}}{\partial x}\right\rangle\right]\left[1 \pm \frac{1}{\left(\frac{3}{2}+2\left\langle\frac{j_n}{j_{n0}}\right\rangle^2\right)}\right] = \pm\frac{F}{2RT}\left[\begin{array}{l}\frac{I(t)}{\kappa_{2n}} - \left(1+\frac{\sigma_{1n}}{\kappa_{2n}}\right)\frac{I(t)}{\sigma_{1n}}\frac{e^{d_{n1}}}{-1+e^{d_{n1}}}\left(1-\frac{1-e^{-d_{n1}}}{d_{n1}}\right) \\ -2\Theta\left\langle\frac{\partial \ln c_2}{\partial x}\right\rangle - \left\langle\frac{\partial U_n}{\partial x}\right\rangle\end{array}\right] \quad [53]$$

In order to retain analytical tractability, we replace the variables with the respective volume averages for the second term in LHS. Hence using Eq. 5 and Eq. 23:

$$\left\langle\frac{j_n}{j_{n0}}\right\rangle^2 = \frac{I(t)^2}{(F a_n l_n k_n)^2\left(c_{sn\max} - \bar{c}_n\right)\bar{c}_n c_{20}} = \left(\frac{I(t)}{I_{n0}}\right)^2 \quad [54]$$

where $(I_{n0})^2 = (F a_n l_n k_n)^2 (c_{sn\max} - \bar{c}_n)\bar{c}_n c_{20}$.

As the volume average of surface concentration is not defined, it is also replaced with the average concentration. Thus:

$$\Rightarrow d_{n1} = \pm \frac{F l_n}{2RT}\left[\frac{I(t)}{\kappa_{2n}} - \left(1+\frac{\sigma_{1n}}{\kappa_{2n}}\right)\frac{I(t)}{\sigma_{1n}}\frac{(d_{n1}-1)\,e^{d_{n1}}+1}{d_{n1}\left(-1+e^{d_{n1}}\right)} - \frac{2\Theta}{l_n}\ln\frac{c_{2in}}{c_{2cc}} - \frac{U_n|_{x=l_n} - U_n|_{x=0}}{l_n}\right] \Bigg/ \left[1 \pm \frac{1}{\left(\frac{3}{2}+2\left(\frac{I}{I_{n0}}\right)^2\right)}\right] + \ln\frac{j_{n0}|_{x=l_n}}{j_{n0}|_{x=0}} \quad [55]$$

Typical values of the parameters for any electrode ($k = n, p$) to get a scale for j_{k0} can be obtained from the following:

$$[j_{k0}] \sim k_k\sqrt{(c_{sk\max} - [c_{sk}])\,[c_{sk}][c_2]} \quad [56]$$

where $\theta = c_{sk}/c_{sk\max}$.

Typical reported[27,29,45] values are $k_k \sim 10^{-11}$ mol$^{-0.5}$ m$^{2.5}$ s^{-1}, $c_{skmax} \sim 25000$ mol m^{-3} and $[c_2] \sim c_{20} \sim 1000$ mol m^{-3}. The state of charge (θ) can be assumed to vary in the range of 0.01 to 0.99. Substituting these values in the above results in

$$[j_{k0}] \sim \sqrt{\theta - \theta^2} \times 10^{-5}\text{mol m}^{-2}\,\text{s}^{-1}$$

The scale for j_{k0} is then taken as the average value and hence

$$[j_{k0}] \sim 5 \times 10^{-6}\text{mol m}^{-2}\,\text{s}^{-1}$$

The scale for j_k is given as

$$[j_k] \sim \frac{I(t)}{a_n F l_n}$$

Using typical reported[45] values of $a_n \sim 10^5$m^{-1} and $l_n \sim 10^{-4}$m, for a standard current density of ~20 A m^{-2} the scale of j_k is evaluated as below.

$$[j_k] \sim 2 \times 10^{-5}\text{mol m}^{-2}\,\text{s}^{-1}$$

Thus, $[j_k]$ is approximately one order larger than $[j_{k0}]$ suggesting for higher over-potentials

Under these scenarios,

$$\left[1 \pm \frac{1}{\left(\frac{3}{2}+2\left(\frac{I}{I_{n0}}\right)^2\right)}\right] \approx 1 \quad [57]$$

The equations for d_{n1} reduces to :

$$\Rightarrow d_{n1} = \pm\frac{F l_n}{2RT}\left[\begin{array}{l}\frac{I(t)}{\kappa_{2n}} - \left(1+\frac{\sigma_{1n}}{\kappa_{2n}}\right)\frac{I(t)}{\sigma_{1n}}\frac{(d_{n1}-1)e^{d_{n1}}+1}{d_{n1}\left(-1+e^{d_{n1}}\right)} \\ -\frac{2\Theta}{l_n}\ln\frac{c_{2in}}{c_{2cc}} - \frac{U_n|_{x=l_n} - U_n|_{x=0}}{l_n}\end{array}\right] + \ln\frac{j_{n0}|_{x=l_n}}{j_{n0}|_{x=0}} \quad [58]$$

Let us define

$$f(d_{n1}) = \frac{(d_{n1}-1)\,e^{d_{n1}}+1}{d_{n1}\left(-1+e^{d_{n1}}\right)} \quad [59]$$

The function $f(d_{n1})$ is bound between 0.5 ($d_{n1} \to 0$) to 1 ($d_{n1} \to \infty$);

$$\lim_{d_{n1}\to 0} f(d_{n1}) = 0.5 \text{ and } \lim_{d_{n1}\to\infty} f(d_{n1}) = 1 \quad [60]$$

Therefore, we could get its value from the previous solution and Eq. 58 can be solved explicitly for d_{n1} as in the current form. For small values of d_{n1}, we can write

$$d_{n1} \sim \pm\frac{F l_n}{2RT}\left[\frac{I(t)}{2\kappa_{2n}} - \frac{I(t)}{2\sigma_{1n}} - \frac{2\Theta}{l_n}\ln\frac{c_{2in}}{c_{2cc}} - \frac{U_n|_{x=l_n} - U_n|_{x=0}}{l_n}\right] + \ln\frac{j_{n0}|_{x=l_n}}{j_{n0}|_{x=0}} \quad [61]$$

Positive electrode.—Substituting for j_p from Eq. 22 and $\partial\Phi_1/\partial x$ from Eq. 34 from solid current balance in Eq. 51 results in

$$\left[-\frac{d_{p1}}{l_p} - \frac{\partial \ln j_{p0}}{\partial x}\right]\left[1 - \frac{1}{\left(\frac{3}{2}+2\left(\frac{j_p}{j_{p0}}\right)^2\right)}\right] = \pm\left(-\frac{F}{2RT}\right)\left[\begin{array}{l}\frac{I(t)}{\kappa_{2p}} - \left(1+\frac{\sigma_{1p}}{\kappa_{2p}}\right)\frac{I(t)}{\sigma_{1p}}\frac{e^{d_{p1}}}{-1+e^{d_{p1}}}\left(1 - e^{\left(-d_{p1}+\frac{d_{p1}(L-x)}{l_p}\right)}\right) \\ -2\Theta\frac{\partial \ln c_2}{\partial x} - \frac{\partial U_p}{\partial x}\end{array}\right] \quad [62]$$

where the positive and negative sign on the RHS are for discharge and charge, respectively. Volume averaging both sides of the above equation gives

$$\left[\frac{d_{p1}}{l_p} + \left\langle\frac{\partial \ln j_{p0}}{\partial x}\right\rangle\right]\left[1 - \frac{1}{\left(\frac{3}{2}+2\left(\frac{I}{I_{p0}}\right)^2\right)}\right] = \pm\frac{F}{2RT}\left[\frac{I(t)}{\kappa_{2p}} - \left(1+\frac{\sigma_{1p}}{\kappa_{2p}}\right)\frac{I(t)}{\sigma_{1p}}\frac{e^{d_{p1}}}{-1+e^{d_{p1}}}\left(1 - \frac{1-e^{-d_{p1}}}{d_{p1}}\right) - 2\Theta\left\langle\frac{\partial \ln c_2}{\partial x}\right\rangle - \left\langle\frac{\partial U_p}{\partial x}\right\rangle\right] \quad [63]$$

$$\Rightarrow d_{p1} = \pm\frac{F l_p}{2RT}\left[\begin{array}{l}\frac{I(t)}{\kappa_{2p}} - \left(1+\frac{\sigma_{1p}}{\kappa_{2p}}\right)\frac{I(t)}{\sigma_{1p}}\frac{(d_{p1}-1)\,e^{d_{p1}}+1}{d_{p1}\left(-1+e^{d_{p1}}\right)} \\ -\frac{2\Theta}{l_p}\ln\frac{c_{2cc}}{c_{2ip}} - \frac{U_p|_{x=L} - U_p|_{x=l_n+l_s}}{l_p}\end{array}\right] \Bigg/ \left[1 \pm \frac{1}{\left(\frac{3}{2}+2\left(\frac{I}{I_{p0}}\right)^2\right)}\right] - \ln\frac{j_{p0}|_{x=L}}{j_{p0}|_{x=l_n+l_s}} \quad [64]$$

Similar to the negative electrode,

$$(I_{p0})^2 = \left(F a_p l_p k_p\right)^2 \left(c_{sp\max} - \bar{c}_p\right)\bar{c}_p c_{20}$$

That further reduces to:

$$\Rightarrow d_{p1} \sim \pm\frac{Fl_p}{2RT}\left[\frac{I(t)}{\kappa_{2p}} - \left(1+\frac{\sigma_{1p}}{\kappa_{2p}}\right)\frac{I(t)}{\sigma_{1p}}\frac{\left(d_{p1}-1\right)e^{d_{p1}}+1}{d_{p1}\left(-1+e^{d_{p1}}\right)} - \frac{2\Theta}{l_p}\ln\frac{c_{2cc}}{c_{2ip}} - \frac{U_p\big|_{x=L} - U_p\big|_{x=l_n+l_s}}{l_p}\right] - \ln\frac{j_{p0}\big|_{x=L}}{j_{p0}\big|_{x=l_n+l_s}} \quad [65]$$

we have

$$f(d_{p1}) = \frac{\left(d_{p1}-1\right)e^{d_{p1}}+1}{d_{p1}\left(-1+e^{d_{p1}}\right)} \quad [66]$$

The function $f(d_{p1})$ is bound between 0.5 ($d_{p1}\to 0$) to 1 ($d_{p1}\to\infty$) as shown earlier; so we can take it from the previous solution to evaluate d_{p1} (Eq. 65) in an explicit simulation scheme. For small values of d_{p1}, we can write

$$\Rightarrow d_{p1} \sim \pm\frac{Fl_p}{2RT}\left[\frac{I(t)}{2\kappa_{2p}} - \frac{I(t)}{2\sigma_{1p}} + \frac{2\Theta}{l_p}\ln\frac{c_{2ip}}{c_{2cc}} - \frac{U_p\big|_{x=L} - U_p\big|_{x=l_n+l_s}}{l_p}\right] + \ln\frac{j_{p0}\big|_{x=l_n+l_s}}{j_{p0}\big|_{x=L}} \quad [67]$$

Electrolyte phase concentration profiles.—*Profile approximations.*—The quasi-steady state solution for the mass balance equation with no source term is a concentration profile linear in space. When a uniform source term is added, the concentration profile becomes quadratic. Therefore, for a spatially varying source term the concentration profile must be of higher order. Based on this general observations, the concentration profiles in both the electrodes are assumed to be third order polynomials. Thus, we have at the negative electrode:

$$c_2(x,t) = n_0(t) + n_1(t)\left(l_n - x\right) + n_2(t)\left(l_n^2 - x^2\right) + n_3(t)\left(l_n^3 - x^3\right) \quad [68]$$

Similarly, at the positive electrode

$$c_2(x,t) = p_0(t) + p_1(t)\left(l_p - (L-x)\right) + p_2(t)\left(l_p^2 - (L-x)^2\right) + p_3(t)\left(l_p^3 - (L-x)^3\right) \quad [69]$$

In the separator, there is no source term in the Li concentration equation for electrolyte phase as no reaction takes place here. The quasi-steady state solution to such condition would be a linear concentration profile. However, linear profile in inadequate for an unsteady process, as it leaves no term to balance the temporal variation. Therefore, a second order concentration profile is required, whereby the coefficient of the quadratic term would balance the transient term of the unsteady species transport equation. Since, battery operation is an unsteady process, the concentration profile in the separator is approximated by a second order polynomial as the following:

$$c_2(x,t) = s_0(t) + s_1(t)\left(x - l_n\right) + s_2(t)(x-l_n)^2 \quad [70]$$

Estimation of polynomial coefficients.—The volume averaged electrolyte balance equations for the electrodes are given as follows[32]

$$\varepsilon_{2n}l_n\frac{\partial\langle c_2\rangle_n}{\partial t} = D_{2n}\frac{\partial c_2}{\partial x}\bigg|_{x=l_n} + a_n(1-t_+)l_n\langle j_n\rangle \quad [71]$$

$$\varepsilon_{2p}l_p\frac{\partial\langle c_2\rangle_p}{\partial t} = -D_{2p}\frac{\partial c_2}{\partial x}\bigg|_{x=l_n+l_s} + a_p(1-t_+)l_p\langle j_p\rangle \quad [72]$$

The above equations are required in the estimation of polynomial coefficients which is performed below.

Applying zero flux boundary condition at the current collector surfaces gives

$$n_1(t) = 0 \text{ and } p_1(t) = 0 \quad [73]$$

Applying the interfacial concentration continuity at the electrode-separator interfaces gives

$$s_0(t) = n_0(t) \quad [74]$$

$$p_0(t) = s_2(t)l_s^2 + s_1(t)l_s + n_0(t) \quad [75]$$

The flux continuity at the negative electrode – separator interface gives

$$D_{2n}\left[-2n_2(t)l_n - 3n_3(t)l_n^2\right] = D_{2s}\left[2s_2(t)l_n + s_1(t)\right] \quad [76]$$

Similarly, the flux continuity at the positive electrode – separator interface gives

$$D_{2p}\left[2p_2(t)l_p + 3p_3(t)l_p^2\right] = D_{2s}\left[2s_2(t)\left(l_n+l_s\right) + s_1(t)\right] \quad [77]$$

The volume averaged concentration in the two electrodes based on the profile approximation can be obtained as

$$\langle c_2\rangle_n = n_0 + \frac{2n_2(t)l_n^2}{3} + \frac{3n_3(t)l_n^3}{4} \quad [78]$$

$$\langle c_2\rangle_p = p_0 + \frac{2p_2(t)l_p^2}{3} + \frac{3p_3(t)l_p^3}{4} \quad [79]$$

$$\langle c_2\rangle_s = s_0 + \frac{2s_2(t)l_s^2}{3} + \frac{s_1(t)l_s}{2} \quad [80]$$

An overall electrolyte balance holds at any time

$$l_n\varepsilon_{2n}\langle c_2\rangle_n + l_s\varepsilon_{2s}\langle c_2\rangle_s + l_p\varepsilon_{2p}\langle c_2\rangle_p = \left(l_n\varepsilon_{2n} + l_s\varepsilon_{2s} + l_p\varepsilon_{2p}\right)c_{20} \quad [81]$$

The volume averaged electrolyte phase mass balance equation for the two electrodes is

$$\varepsilon_{2n}\frac{\partial\langle c_2\rangle_n}{\partial t} = -D_{2n}\left(2n_2(t) + 3n_3(t)l_n\right) + a_n(1-t_+)\langle j_n\rangle \quad [82]$$

$$\varepsilon_{2p}\frac{\partial\langle c_2\rangle_p}{\partial t} = -D_{2p}\left(2p_2(t) + 3p_3(t)l_p\right) + a_p(1-t_+)\langle j_p\rangle \quad [83]$$

So far, we have a total of 14 unknowns, i.e., $n_0(t)$, $n_1(t)$, $n_2(t)$, $n_3(t)$, $p_0(t)$, p_1(t), $p_2(t)$, $p_3(t)$, $s_0(t)$, $s_1(t)$, $s_2(t)$, $<c_2>_n$, $<c_2>_p$, $<c_2>_s$ but only 12 equations (Eqs. 73–83). On the other hand, the above equations do not invoke the effects of spatial variation of the reaction rates as well. In this regard, we write local mass balance equations at $x = 0$ and L for the assumed concentration and reaction rate profiles:

$$\varepsilon_{2n}\frac{\partial c_2|_{x=0}}{\partial t} = -2D_{2n}n_2(t) + a_n(1-t_+)j_n|_{x=0} \quad [84]$$

$$\varepsilon_{2p}\frac{\partial c_2|_{x=L}}{\partial t} = -2D_{2p}p_2(t) + a_p(1-t_+)j_p\big|_{x=L} \quad [85]$$

From the profile approximations, we can also write

$$c_2|_{x=0} = n_2(t)l_n^2 + n_3(t)l_n^3 + n_0 \quad [86]$$

$$c_2|_{x=L} = p_2(t)l_p^2 + p_3(t)l_p^3 + p_0 \quad [87]$$

Now, we have 2 additional unknowns: $c_2|_{x=0}$ and $c_2|_{x=\mathrm{L}}$ and thus, a total of 16 unknowns. We also have 16 equations (Eqs. 73–87) – 4 ODEs and 12 algebraic equations.

Solid phase surface concentration.—With the quartic profile approximation for the solid state diffusion, the surface concentration can be resolved with the equations below:[46]

$$c_{sk} = \bar{c}_{1k} - \frac{r_k}{35D_{1k}}j_k + \frac{8r_k}{35}\bar{c}_{1kr} \quad [88]$$

$$\frac{d\bar{c}_{1k}}{dt} = -\frac{3j_k}{R_k} \quad [89]$$

$$\frac{d\,\bar{c}_{1rk}}{dt} + \frac{30D_{1n}\bar{c}_{1rk}}{R_k^2} = -\frac{45j_k}{2R_k^2} \quad [90]$$

where $\bar{c}_{1k}$ and $\bar{c}_{1rk}$ are the sphere average concentration and sphere average radial gradient of concentration, r_k is the radii of active material spheres, and D_{1k} is the solid phase diffusivity. The two ODEs in the above are subject to the following initial conditions:

$$\bar{c}_{1k}(r,0) = c_{1k0} \quad [91]$$

$$\bar{c}_{1rk}(r,0) = 0 \quad [92]$$

Note that a relatively simple model for the solid phase diffusion[46] is considered here to demonstrate the utility of the proposed model reduction approach, i.e., NUROM. This model has been found to be efficient at long time ranges and for low/medium rates. However, it might not be adequate for high rate applications. Several improved models for solid phase diffusion are available in the literature[47–53] and could be opted for better accuracy at high rates.

Cell voltage.—The cell voltage is the solid phase potential difference between the two collector ends.

$$V_{cell} = \Phi_1(x=L) - \Phi_1(x=0) \quad [93]$$

From the inverted Butler-Volmer equation, we have

$$\Phi_1 = U_k + \Phi_2 + \frac{2RT}{F}\sinh^{-1}\left(\frac{j_k}{j_{k0}}\right) \quad [94]$$

Substituting the above in the expression for cell voltage gives

$$V_{cell} = \left(U_p + \Phi_2 + \frac{2RT}{F}\sinh^{-1}\left(\frac{j_p}{j_{p0}}\right)\right)\Big|_{x=L} - \left(U_n + \Phi_2 + \frac{2RT}{F}\sinh^{-1}\left(\frac{j_n}{j_{n0}}\right)\right)\Big|_{x=0} \quad [95]$$

Substituting for $\Phi_2\,(x=L,\,t)$ and $\Phi_2\,(x=0,\,t)$ from Eq. 43 and 41 in the above gives

$$V_{cell} = \left[U_p(L,t) + \Phi_{2ip}(t) + 2\Theta\ln\left(\frac{c_2(L,t)}{c_{2ip}(t)}\right) - \frac{I(t)l_p}{\kappa_{2p}}\left(1-f(d_{p1})\right) + \frac{2RT}{F}\sinh^{-1}\left(\frac{j_p(L,t)}{j_{p0}(L,t)}\right)\right] - \left[U_n(0,t) + \Phi_{2in}(t) + 2\Theta\ln\left(\frac{c_2(0,t)}{c_{2in}(t)}\right) + \frac{I(t)l_n}{\kappa_{2n}}\left(1-f(d_{n1})\right) + \frac{2RT}{F}\sinh^{-1}\left(\frac{j_n(0,t)}{j_{n0}(0,t)}\right)\right] \quad [96]$$

Substituting for Φ_{2ip} and Φ_{2in} from Eq. 36 and 37 in the above gives

$$V_{cell} = U_p(L,t) - U_n(0,t) + \frac{2RT}{F}\sinh^{-1}\left(\frac{j_p(L,t)}{j_{p0}(L,t)}\right) - \frac{2RT}{F}\sinh^{-1}\left(\frac{j_n(0,t)}{j_{n0}(0,t)}\right) + 2\Theta\left[\ln\left(\frac{c_{2ip}(t)}{c_{2mid}(t)}\right) + \ln\left(\frac{c_2(L,t)}{c_{2ip}(t)}\right)\right] - 2\Theta\left[\ln\left(\frac{c_{2in}(t)}{c_{2mid}(t)}\right) + 2\Theta\ln\left(\frac{c_2(0,t)}{c_{2in}(t)}\right)\right] - \frac{I(t)l_s}{\kappa_{2s}} - \frac{I(t)l_p}{\kappa_{2p}}\left(1-f(d_{p1})\right) - \frac{I(t)l_n}{\kappa_{2n}}\left(1-f(d_{n1})\right) \quad [97]$$

Gathering all the logarithmic terms, the above can be rewritten as

$$V_{cell} = U_p(L,t) - U_n(0,t) + \frac{2RT}{F}\sinh^{-1}\left(\frac{j_p(L,t)}{j_{p0}(L,t)}\right)$$

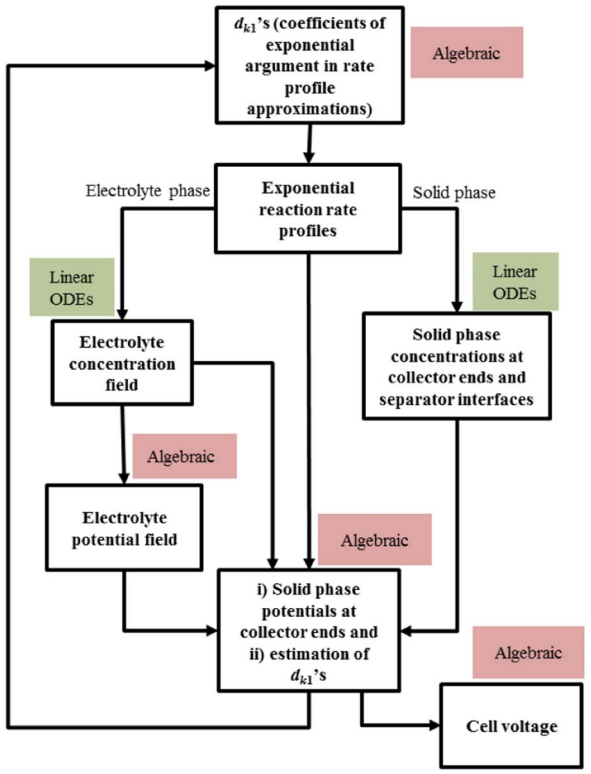

Figure 1. Schematic of the model for cell voltage prediction.

$$-\frac{2RT}{F}\sinh^{-1}\left(\frac{j_n(0,t)}{j_{n0}(0,t)}\right) - \frac{I(t)l_s}{\kappa_{2s}} - \frac{I(t)l_p}{\kappa_{2p}}\left(1-f(d_{p1})\right) - \frac{I(t)l_n}{\kappa_{2n}}\left(1-f(d_{n1})\right) + 2\Theta\ln\left(\frac{c_2(L,t)}{c_2(0,t)}\right) \quad [98]$$

Simulation Algorithm

We follow a sequential simulation algorithm for the NUROM framework which is presented in a flow chart (Fig. 1). Reaction rates and solid current profiles at time $t=0$, all the points in the electrode are at same solid and electrolyte concentrations. Therefore, d_{k1}'s at $t=0$ are given as

$$d_{n1}(t=0) \sim \pm\frac{Fl_n}{2RT}\left[\frac{I(t)}{2\kappa_{2n}} - \frac{I(t)}{2\sigma_{1n}}\right] \quad [99]$$

$$d_{p1}(t=0) \sim \pm\frac{Fl_p}{2RT}\left[\frac{I(t)}{2\kappa_{2p}} - \frac{I(t)}{2\sigma_{1p}}\right] \quad [100]$$

Once the values of d_{k1}'s are known, we can get the reaction rate profiles from Eqs. 21–22. For the given exponential profiles, the solid current profiles in the negative and positive electrodes are obtained by Eqs. 31 and 34, respectively.

Electrolyte concentration field.—The electrolyte concentration field is approximated as the polynomial expressions given by Eqs. 68–70. The polynomial coefficients are estimated by solving the system of 4 ODEs and 12 linear algebraic equations (Eqs. 73–87). For computing the cell voltage, the electrolyte concentrations at the current collector ends are needed which are obtained from Eqs. 86 and 87.

Electrolyte potential field.—The electrolyte potential field in the electrodes is expressed in terms of the electrode-separator interfacial potentials. In this work zero reference potential is set in the middle of the separator. The interfacial electrolyte potentials are computed

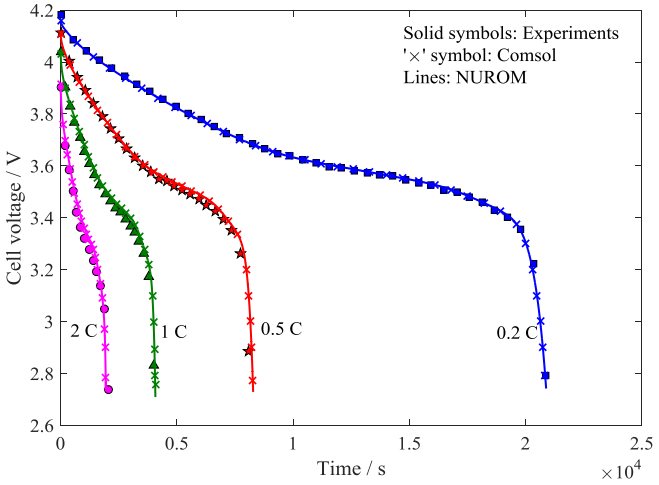

Figure 2. Cell voltage validation against experimental results.[45]

from Eqs. 36 and 37. Note that these equations require the interfacial and mid-separator electrolyte concentrations. The electrolyte potential at the collector ends are computed using these interfacial electrolyte potentials using Eqs. 41 and 43. The electrolyte potential profiles in the three regions are computed using Eqs. 35, 40 and 42. These internal profiles are not required for cell voltage computation.

Solid phase concentration at collector ends and separator interfaces.—Quartic profile approximation expresses the concentration profile within an active material sphere in terms of average concentration and the average radial gradient. The coupled ODEs, Eqs. 89–90, are solved with initial conditions Eqs. 91–92 at two points, i.e., the collector end and the separator interface for each electrode. The surface concentration at all the four points is obtained by Eq. 88. With the same procedure, we can estimate the surface concentration at other points in the two electrodes; however, these are not required for cell voltage computation.

Cell voltage.—The cell voltage is given as the difference in solid phase potentials at the two collector ends.

In the electrolyte phase, the electrolyte concentration field is resolved first through the solution of Eqs. 73–87, which then enables the solution of the electrolyte potential field. In the solid phase, the solid phase concentration field is solved. All the above fields provide input for the Butler-Volmer kinetics to solve for the solid potential field. Eventually, the cell voltage is computed as the solid phase potential difference between the two collector ends Eq. 97. The unknowns, d_{k1}'s are computed at the end (Eqs. 61 and 67) which are then fed back to the reaction rate expression for the next time step.

Results and Discussion

Validation with experimental results and full model.—The model predictions using the NUROM formulation are compared with those from experimental results and detailed electrochemical model in COMSOL for a typical commercial cell prismatic LMO-graphite cell of 11.5Ah capacity.[45] The detail cell parameters could be found in Ref. 45. The open circuit potentials and experimentally predicted voltage at different discharge rates at room temperature are digitally retrieved from the same reference. The cell model is recreated in COMSOL Li-ion battery model for validation and comparison also. The NUROM at present is an isothermal model. At room temperature (298 K), the model is run at different discharge rates (0.2C, 0.5C, 1.0C and 2.0C). The COMSOL model is run at the same discharge rates as the NUROM model. Cell voltage prediction by NUROM, COMSOL and experimental results are compared in Figure 2. The results show excellent match between the model predictions (COMSOL

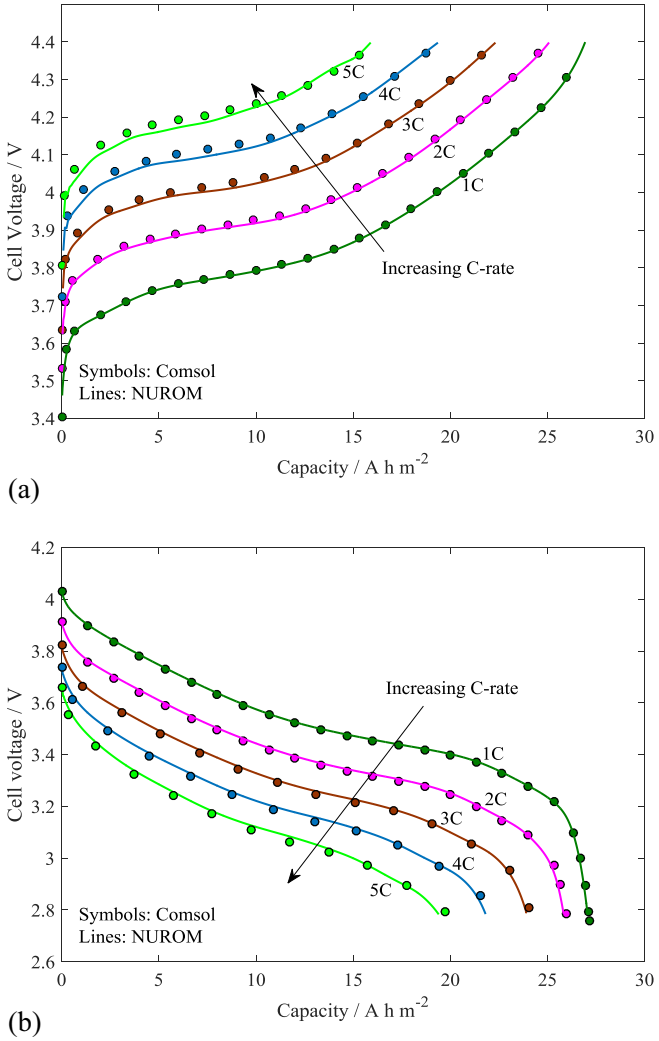

Figure 3. Verification of the present model against COMSOL model (full P2D). (a) constant current charge, (b) constant current discharge.

and NUROM) and experimental measurements. The percentage error ($error = \frac{|V_{mod} - V_{exp}|}{V_{exp}} \times 100$) between experimental result and both the numerical results are less than 1%.

Verification with full model at high discharge rates.—To assess the performance of NUROM at higher rates (1C to 5C), it is compared with COMSOL for both constant current charge and discharge (Figs. 3a and 3b). The NUROM prediction of voltage matches extremely well with COMSOL. Even at high C rate (5C) the mismatch in voltage prediction between COMSOL and NUROM is of the order of 10mV. The percentage error is less than 1%. Thus, it can be concluded that NUROM can predict the voltage with same accuracy as full P2D model for a wide range of charge/discharge rate (0.2C–5.0C) at room temperature. This range would cover most of the possible operating conditions of all Li-ion battery powered equipment including the electric vehicle. Typically, in reduced order models additional corrections (eg. State estimators) are added to achieve high accuracy. For the present model, high accuracy can be achieved without any additional correction.

Analysis and comparison of internal variables.—*Discharge at 1C rate.*—The internal parameters of the cell are monitored and compared with COMSOL results to ascertain the efficacy of the present model. If the predictions of the internal variables match between NUROM and COMSOL based full model, it can be concluded that the NUROM

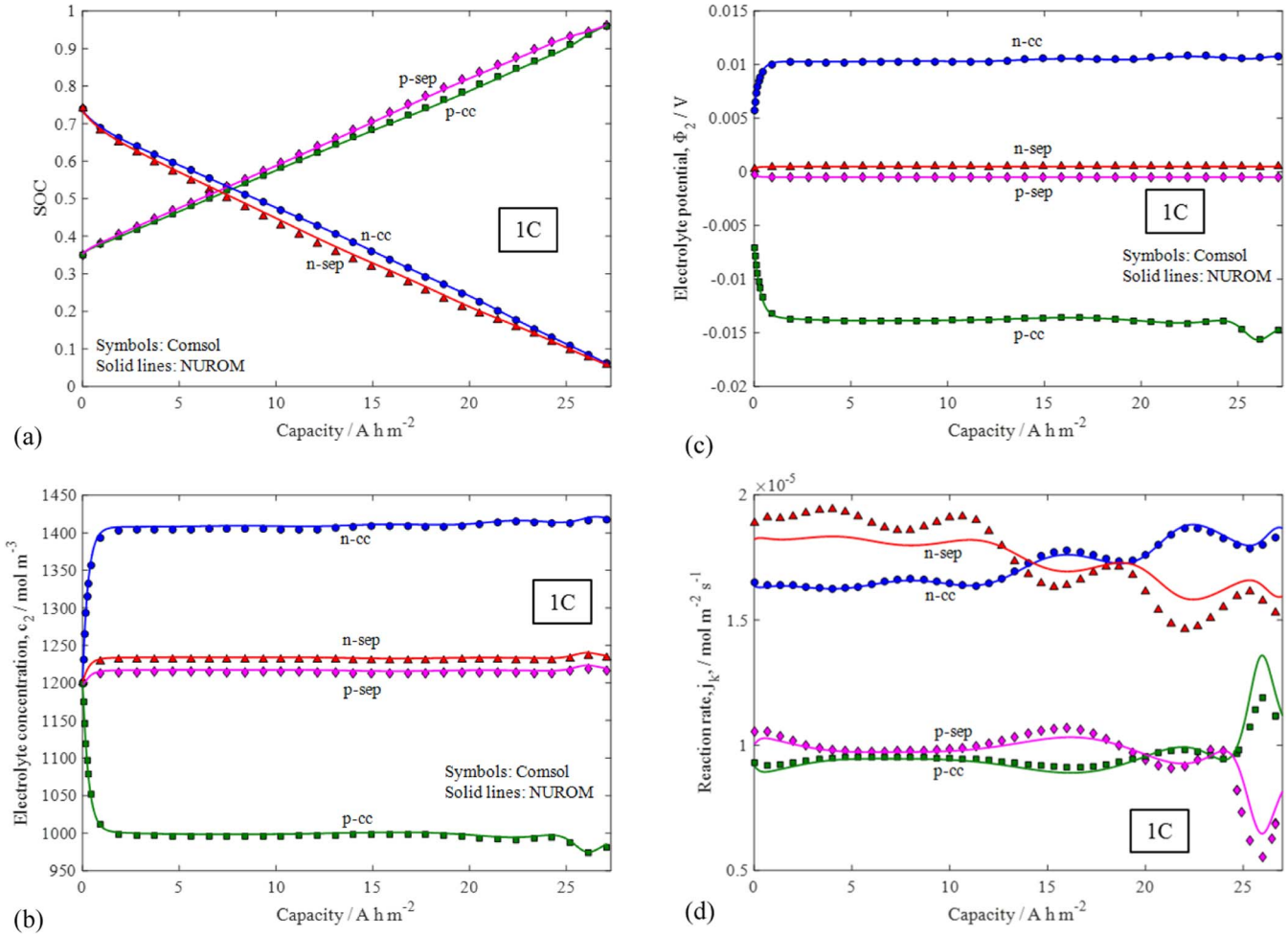

Figure 4. Comparison of present model with COMSOL at 1C discharge for four points: n-cc (anode current collector end), n-sep (anode separator end), p-sep (cathode separator end), p-cc (cathode current collector end). (a) SOC, (b) Electrolyte concentration, (c) electrolyte potential (d) reaction rate.

effectively mimics the physical processes inside the cell with low computational cost. For 1C constant current discharge, the comparison is shown in Fig. 4. The electrode SOCs at both the ends (separator end and current collector end) are plotted in Fig. 4a. As the cell is able to sustain 5C discharge (Fig. 3), it is expected to be a power cell. Thus, at moderate discharge rates like 1C, the reaction rate is expected to be close to uniform. The same can be seen in Fig. 4d. The reaction rate at anode separator is about 1.8×10^5 mol.m^{-2}.s^{-1} at the beginning of discharge while the same is 1.6×10^5 mol.m^{-2}.s^{-1} at the anode current collector. Reaction rate is slightly greater near the separator due to the high electronic conductivity of graphite compared to Li-ion conductivity of electrolyte. In other words, resistance to Li-ion transport across the anode is greater than resistance to electron transport across the anode. For discharge reaction at the anode current collector end, the de-intercalated Li-ion from graphite needs to be transported across the anode. For the same reaction at the anode separator end, the electrons needs to be transported across the anode. As a result, there is more reaction where the resistance is lesser, i.e., at the separator end. However, due to greater reaction rate at the separator end, local anode OCP at anode separator becomes greater than anode current collector. As a result, resistance to reaction increases there and the rate of reaction increases at the current collector end as the discharge progresses. At about 14Ah.m^{-2} capacity, the reaction rates at both ends are same (Fig. 4d). At the same point, the difference in anode SOC between separator and current collector is the maximum. Thereafter, the reaction rate at the current collector increases and at the end of the discharge the anode SOC is the same at both separator and current collector. The NUROM result is able to follow the COMSOL results well. Although the reaction rate at the current collector end matches exactly, there is some difference in the anode separator reaction rate.

Similarly, at the cathode side, the SOC at both separator and current collector increase at almost the same rate as the reaction rates at both the points are almost same. However, as the cathode is thicker than anode while the total reaction rate in both the electrodes are equal, the local volumetric reaction rate is lesser in the cathode. Even in the case of cathode, the reaction rate is greater at the separator end than the current collector end, at the beginning of discharge. As the cathode particles fill up the open circuit potential decreases. At about 23Ah.m^{-2} capacity, the cathode SOC at separator end reaches close to 0.9 and a rapid drop in cathode OCP starts there. This results in increased over-potential and thus a sharp drop in reaction rate. To compensate for that, the reaction rate at the current collector end of the cathode increases. NUROM is able to predict this behavior as well as COMSOL (Fig. 4d).

The concentration of Li-ion in the electrolyte phase at the two ends of both the electrodes are plotted in Fig. 4b. Agreement of the NUROM results with COMSOL results is excellent at all points for the complete discharge. This suggests that the cubic profile in the electrodes and quadratic profile in the separator assumed for the Li-ion concentration is adequate at this discharge rate. The Li-ion concentration quickly reaches a constant value at all the four points plotted in Fig. 4b. For constant current discharge condition, it can be concluded that the Li-ion concentration profile in the electrode reaches a quasi-steady state to support the ion transport. At the cathode current collector, diffusive transport of Li-ion approaches zero while the intercalation rate is finite and thus, the Li concentration at the

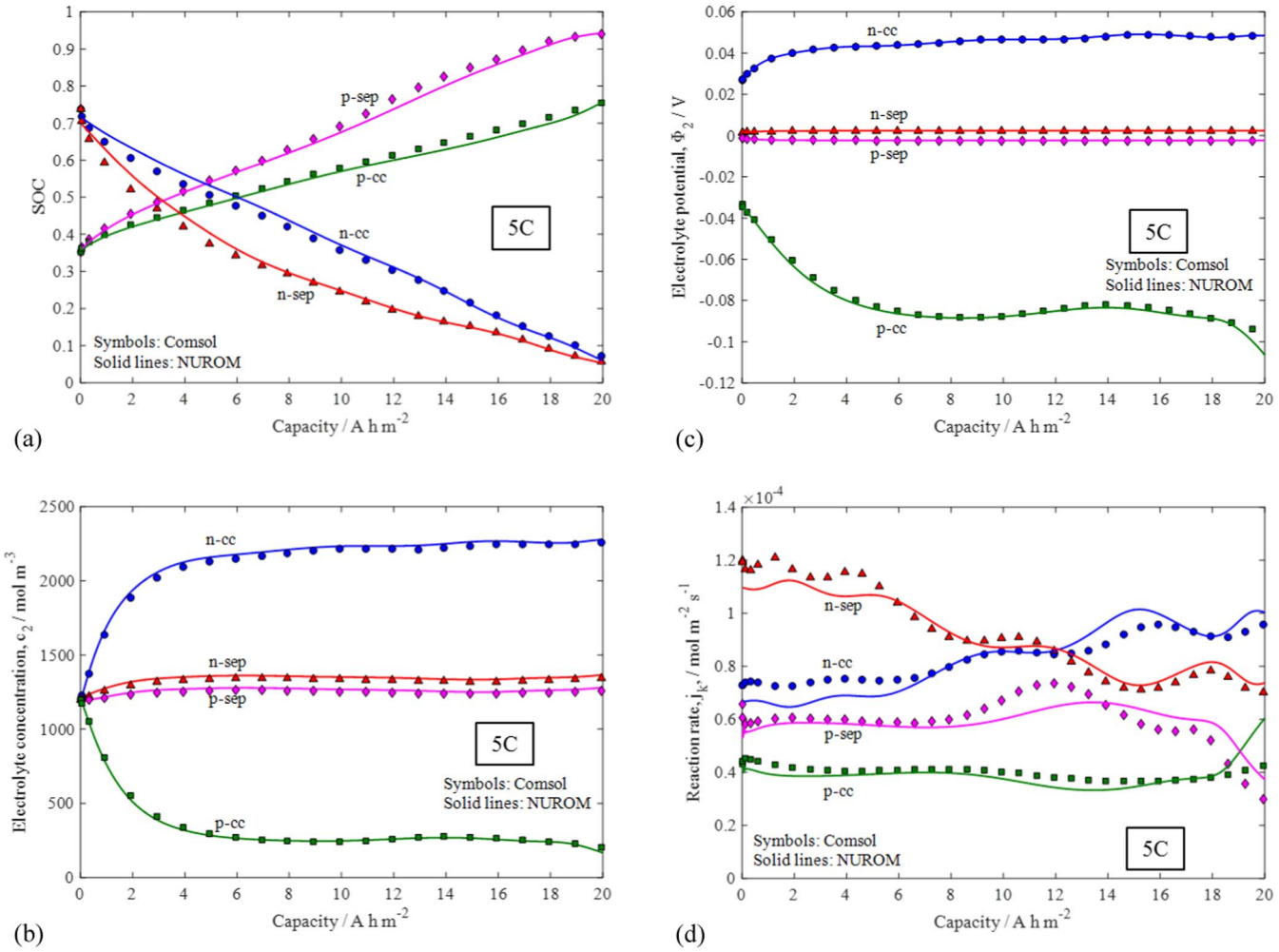

Figure 5. Comparison of present model with COMSOL at 5C discharge for four points: n-cc (anode current collector end), n-sep (anode separator end), p-sep (cathode separator end), p-cc (cathode current collector end). (a) SOC, (b) Electrolyte concentration, (c) electrolyte potential (d) reaction rate.

electrolyte decreases considerably. At the cathode separator, diffusion flux of Li-ion in electrolyte is greater than the intercalation rate and thus the steady state Li-ion concentration is greater than the initial concentration. At the anode separator end, Li-ion diffuses away towards cathode while there is de-intercalation of Li-ion from graphite. As the de-intercalation is greater than the diffusion, the steady state Li-ion concentration is greater than the initial concentration. This difference is much greater at the anode current collector end, as the diffusion flux in electrolyte approaches zero at the current collector. Thus the steady state Li-ion concentration at anode current collector is much greater than the initial concentration. The corresponding electrolyte phase potentials are plotted in Fig. 4c. The initial condition is assumed to be at zero potential and the behavior is proportional to the Li-ion concentration. NUROM and COMSOL results agree perfectly for electrolyte potential.

Discharge at 5C rate.—The internal variables are compared between NUROM and COMSOL at 5C discharge condition at the same four points in Fig. 5. There is qualitative match in anode SOC (maximum difference in predictions by NUROM and COMSOL is less than 3%) evolution (Fig. 5a) and reaction rates (Fig. 5d). However, the NUROM calculated reactions rates are slightly lesser compared to the COMSOL calculated reactions rates in the anode at the beginning of discharge (Fig. 5d). As a result, NUROM predicts slightly lesser drop in anode SOC at the beginning of discharge compared to COMSOL. After about 12Ah.m^{-2} capacity, the anode reaction rate prediction by NUROM is slightly greater than COMSOL at the current collector and separator. Thus, the anode SOC matched perfectly between COMSOL and NUROM by the end of discharge (Fig. 5a). In the cathode side, there is a similar qualitative match (Fig. 5a and Fig. 5d). However, at this high discharge rate, the cathode SOCs at the separator and current collector are do not come back to a constant value at the end of discharge. The COMSOL and NUROM prediction of cathode SOC is very good for the complete discharge (Fig. 5a). At this high discharge rate, difference in reaction rate between separator and current collector at the cathode is greater (Fig. 5d). As the local cathode SOC at separator reaches close to 0.9 at around 18Ah.m^{-2} (Fig. 5a), the reaction rate drops drastically (Fig. 5d), which is similar to 1C discharge condition. On the other hand, the reaction rate at the current collector peaks up. This behavior is captured by NUROM, although the exact location of drop or rise in reaction rates have slight mismatch with COMSOL. Before the cathode SOCs could be equilibrated, the discharge cut-off voltage is reached (Fig. 5a). There is excellent agreement in SOC prediction between NUROM and COMSOL. The Li-ion concentration in electrolyte is plotted in Fig. 5b. There is qualitative match in the concentration profiles with 1C discharge condition, and the electrolyte concentration levels have a longer transience in this case compared to 1C discharge condition (Fig. 4b). The range of Li-ion concentration across the cell (anode current collector to cathode current collector) in this case is wider. This can be easily explained by the high discharge rate. A larger concentration gradient is required to support greater discharge rate. NUROM and COMSOL predictions of both electrolyte concentration (Fig. 5b) and electrolyte phase potential (Fig. 5c) have almost perfect agreement.

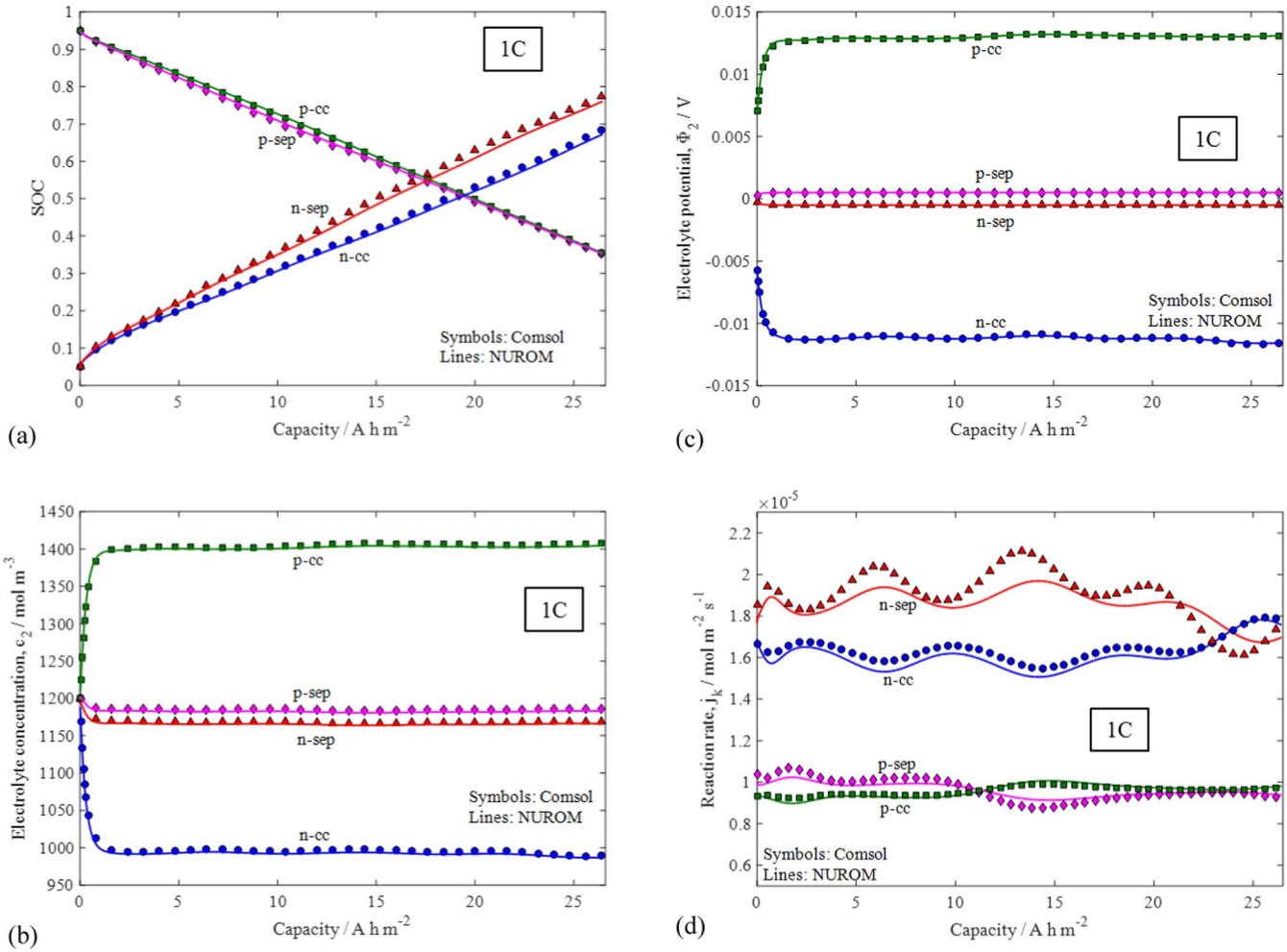

Figure 6. Comparison of present model with COMSOL at 1C charge for four points: n-cc (anode current collector end), n-sep (anode separator end), p-sep (cathode separator end), p-cc (cathode current collector end). (a) SOC, (b) Electrolyte concentration, (c) electrolyte potential (d) reaction rate.

Charge at 1C rate.—The cell internal variables for 1C rate charging is plotted in Fig. 6. During 1C rate charging, the cathode reaction rates at both current collector and separator end are almost equal (Fig. 5d). As a result, cathode SOC at these two points almost coincide (Fig. 5a). COMSOL and NUROM both predict this behavior very well. However, in the anode side reaction rate (intercalation) is greater at the separator than at the current collector. It remains so for till 22Ah.m^{-2} capacity. At this point, the anode SOC at separator reaches 0.7 and there is relatively faster drop in anode OCP, which results in decrease in reaction rate. To compensate for that, the reaction rate at the anode current collector increases. The reaction rate in anode exhibits a sinusoidal pattern (Fig. 6d). NUROM is able to predict the same pattern with a slightly smaller amplitude. The Li-ion concentration in electrolyte and electrolyte phase potentials at the same points are plotted for 1C rate charge condition in Figs. 6b and 6c respectively. The Li-ion concentration quickly reaches a steady state (Fig. 6b) like in the case of 1C rate discharging (Fig. 4b). In this case however, the anode side has lower concentration while the cathode side has higher concentration as the direction of reaction has reversed. In both the cases, NUROM and COMSOL results have perfect agreement.

Charge at 5C rate.—Cell internal variables at 5C rate charge condition is plotted in Fig. 7. Cathode SOC evolution at separator and current collector are close to each other (Fig. 7a) as the reaction rate predictions are almost equal (Fig. 7d). In the first half of charging, reaction rate at cathode separator is greater while in the second half of the charging it is just the opposite. NUROM predictions agree almost perfectly with the COMSOL results. In the anode side, the reaction rate is much greater at the separator side compared to the current collector (Fig. 7d). The reason is that the electronic resistance in graphite is much lower compared to the Li-ion transport resistance in the anode electrolyte phase. NUROM is able to predict the reaction rate well even for this case. However, NUROM under predicts the reaction rate at the anode separator end in the first half and over predicts in the second half (Fig. 7d). The Li-ion concentration in electrolyte and electrolyte phase potentials at these points are plotted in Figs. 7b and 7c respectively. During charging, the current cathode current collector has the maximum Li-ion concentration while the anode current collector has the minimum Li-ion concentration in the electrolyte phase (Fig. 7b). This is consistent with the charging at 1C condition (Fig. 6b). NUROM and COMSOL results agree very well for all four points.

Accuracy, computation time and inferences.—From the analysis of the results it is clear that the present model has the capability to predict the cell voltage as good as the full model for a wide range of operation (0.2C – 5C). The fact that the set of parameters (d_{k1}, d_{k2}) used in reduced order model to achieve cell voltage match may not be unique, casts a lingering doubt about the robustness and applicability of such models. Therefore, evolution of local variables at different locations inside the cell is compared between the present model and the full P2D model (COMSOL). Till 1C rate, the match between NUROM and COMSOL is perfect. At very high rate of 5C, there is small difference

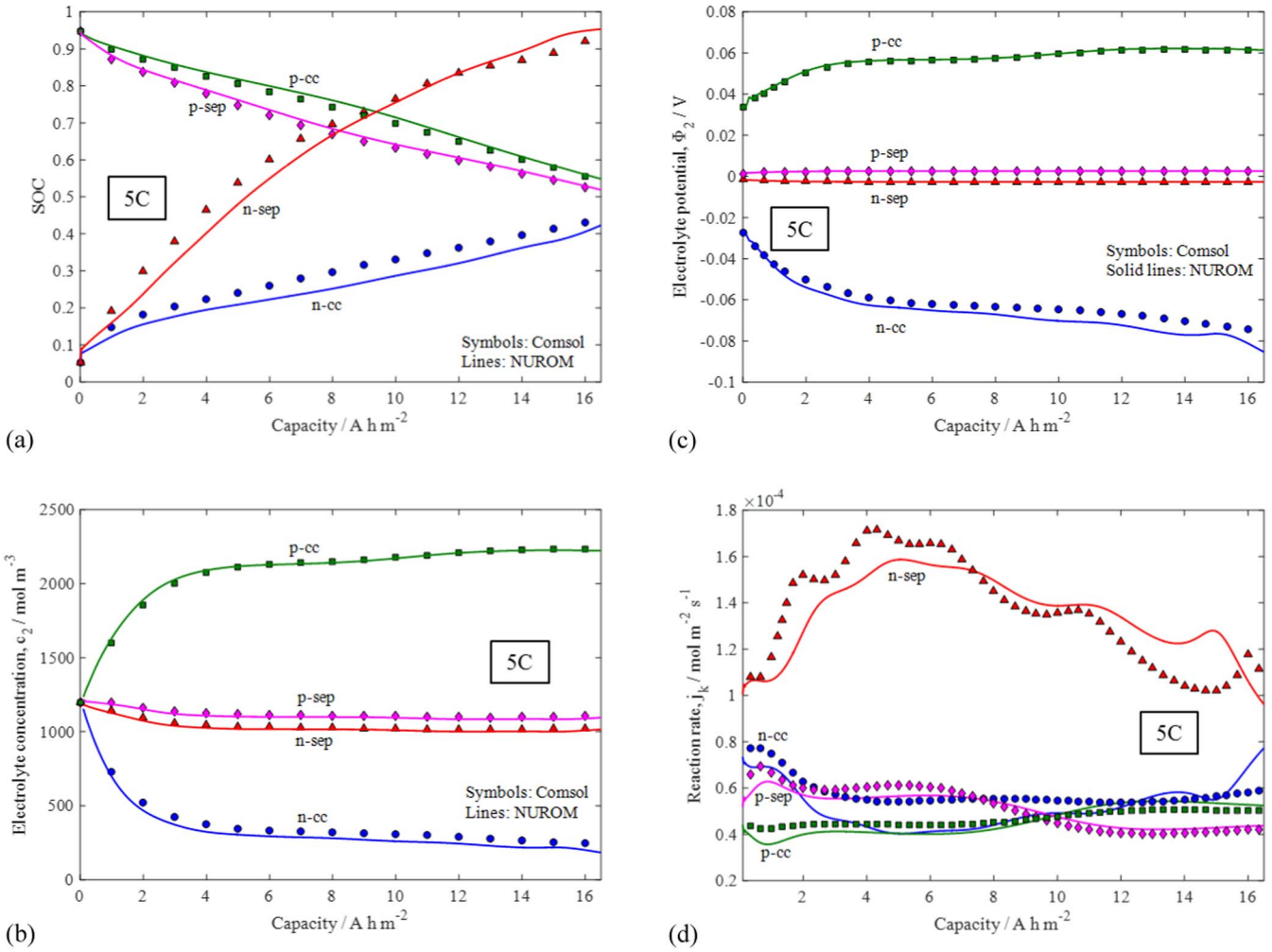

Figure 7. Comparison of present model with COMSOL at 5C charge for four points: n-cc (anode current collector end), n-sep (anode separator end), p-sep (cathode separator end), p-cc (cathode current collector end). (a) SOC, (b) Electrolyte concentration, (c) electrolyte potential (d) reaction rate.

between NUROM and COMSOL estimation of local variables. For 1C discharge solving for around 4000 time steps (interval of 1 s), NUROM takes around 0.6 s on an i7 with 8 GB RAM. Hence, simulation time required for a single time step is around 1.5×10^{-4} s, in suitable range for onboard implementation. Overall, it is concluded that the reaction profile and electrolyte concentration profile assumption used in NUROM is robust and accurate for almost the whole operating range of a Li-ion battery, and the formalism and the ease of computation makes it a fit candidate for onboard state estimation algorithm, in addition to a quick design tool.

Conclusions

There has been a concerted effort to use more reliable physics based model for onboard Li-ion battery management system. However, complex computation of full P2D model for Li-ion battery proved to be a deterrent to that. Although reduced order P2D models are also available, excessive simplification decrease the reliability of these models. This paper presents novel approach of using exponential reaction rate and polynomial Li-ion concentration profile on P2D model which increases the computational efficiency without compromising the reliability of full P2D model. The DAE nature of the model helps in solving for some of the dependent variables analytically. The model reformulation is demonstrated and validated against experimental data for low-to-moderate discharge rates. The model is verified against COMSOL based full P2D model upto high rate (5C) charge and discharge. The predictions of internal variables like local reaction rate, electrode SOC, electrolyte concentration, electrolyte potentials between NUROM and COMSOL show excellent agreement. It can be concluded that the physical processes in the cell are effectively modelled through NUROM and the results are of the same level as full electrochemical model obtained at much lower computational cost. Therefore, NUROM is excellently placed for implementation as onboard state estimation tool in Li-ion battery powered equipment including electric vehicles. The model can be extended further with inclusion of energy equation to work at all temperatures, and consideration of advanced models for solid phase diffusion[47–53] for a better accuracy at high rates.

Appendix: Approximation of Reaction Rate Profiles

A physics-based mathematical model for a Li-ion battery accounting for conservation of charge and species (both in electrolyte and solid phase) typically needs to be solved numerically. Therefore, reaction rate profiles along the thickness of an electrode cannot be predicted a priori simulations. In this regard, the aim is to determine the approximate functional form of reaction rate profiles analytically which is indeed possible with the following assumptions introduced:

1. The cell is isothermal.
2. The diffusion current is negligible as compared to the migration.
3. Linearized form of Butler-Volmer equation governs the kinetics.

$$j_k = j_{k0}\left[\frac{F}{2RT}\left(\Phi_1 - \Phi_2 - U_k\right)\right] \qquad [A1]$$

4. Both electrolyte and solid phase concentrations do not vary along the thickness of an electrode, thus allowing to consider over-potential independent rate pre-factor, j_{k0} to be constant.
5. The electronic and ionic conductivities are constant throughout the thickness of an electrode.

With the above assumptions, we get the following equations for the conservation of charge:

$$\frac{\partial}{\partial x}\left(-\sigma_{1k}\frac{\partial \Phi_1}{\partial x}\right) = -a_k F\, j_k \quad [A2]$$

$$\frac{\partial}{\partial x}\left(-\kappa_{2k}\frac{\partial \Phi_2}{\partial x}\right) = a_k F\, j_k \quad [A3]$$

which is subject to the boundary conditions below:

- At the current collector / electrode interfaces ($x = 0$ *and* $x = L = l_n + l_s + l_p$) :

$$-\kappa_{2k}\frac{\partial \Phi_2}{\partial x} = 0 \quad [A4]$$

$$-\sigma_{1k}\frac{\partial \Phi_1}{\partial x} = I(t) \quad [A5]$$

- At the separator / electrode interfaces ($x = l_n$ *and* $x = l_n + l_s$) :

$$-\kappa_{2k}\frac{\partial \Phi_2}{\partial x} = I(t) \quad [A6]$$

$$-\sigma_{1k}\frac{\partial \Phi_1}{\partial x} = 0 \quad [A7]$$

Setting $\Phi_1 = 0$ at $x = 0$, the above system of coupled second order ordinary differential equations can be solved analytically at any time, t, e.g., at the negative electrode

$$\Phi_1(x,t) = -\frac{I(t)x}{\sigma_{1n}+\kappa_{2n}} + \frac{I(t)\left[\kappa_{2n}\left(-\zeta_1 + \kappa_{2n}\zeta_2(x)\right)\right]}{\sigma_{1n}\kappa_{2n}\zeta_3\lambda_1} \quad [A8]$$

$$\Phi_2(x,t) = -U_n - \frac{I(t)x}{\sigma_{1n}+\kappa_{2n}} - \frac{I(t)\left[\kappa_{2n}\zeta_1 + \sigma_{1n}\zeta_2(x)\right]}{\sigma_{1n}\kappa_{2n}\zeta_3\lambda_1} \quad [A9]$$

where

$$\zeta_1 = 2\sigma_{1n} + \kappa_{2n}\left(e^{\lambda_1 l_n} + e^{-\lambda_1 l_n}\right) \quad [A10]$$

$$\zeta_2(x) = \sigma_{1n}\left(e^{\lambda_1 x} + e^{-\lambda_1 x}\right) + \kappa_{2n}\left(e^{\lambda_1 (l_n - x)} + e^{-\lambda_1 (l_n - x)}\right) \quad [A11]$$

$$\zeta_3 = (\sigma_{1n}+\kappa_{2n})\left(e^{\lambda_1 l_n} - e^{-\lambda_1 l_n}\right) \quad [A12]$$

$$\lambda_1 = \sqrt{\frac{F(\sigma_{1n}+\kappa_{2n})(j_{k0}a_n F)}{RT\sigma_{1n}\kappa_{2n}}} \quad [A13]$$

The above analytical solution, i.e., Eq. A8 (or Eq. A9) can be substituted in the governing equations, i.e., Eq. A2 (or Eq. A3) to find the reaction rate, j_n as function of x:

$$j_n(x,t) = -\frac{1}{a_n F}\frac{\partial}{\partial x}\left(-\sigma_{1n}\frac{\partial \Phi_1}{\partial x}\right) \quad [A14]$$

or

$$j_n(x,t) = \frac{\sigma_{1n}}{a_n F}\left[\frac{I(t)}{\sigma_{1n}\kappa_{2n}\zeta_3\lambda_1}\kappa_{2n}\frac{\partial^2}{\partial x^2}\zeta_2(x)\right] \quad [A15]$$

or

$$j_n(x,t) = \frac{I(t)}{a_n F}\frac{\lambda_1}{(\sigma_{1n}+\kappa_{2n})\left(e^{\lambda_1 l_n} - e^{-\lambda_1 l_n}\right)} \left[\sigma_{1n}\left(e^{\lambda_1 x} + e^{-\lambda_1 x}\right) + \kappa_{2n}\left(e^{\lambda_1 (l_n - x)} + e^{-\lambda_1 (l_n - x)}\right)\right] \quad [A16]$$

or

$$j_n(x,t) = \frac{I(t)}{a_n F l_n}\left[\beta_n\sigma_{1n}\left(e^{\lambda_1 x} + e^{-\lambda_1 x}\right) + \beta_n\kappa_{2n}\left(e^{\lambda_1 (l_n - x)} + e^{-\lambda_1 (l_n - x)}\right)\right] \quad [A17]$$

where

$$\beta_n = \frac{\lambda_1 l_n}{(\sigma_{1n}+\kappa_{2n})\left(e^{\lambda_1 l_n} - e^{-\lambda_1 l_n}\right)} \quad [A18]$$

Since, λ_1, x, (l_n-x) are positive real numbers, $e^{\lambda_1 x} > e^{-\lambda_1 x}$ and $e^{\lambda_1 (l_n - x)} > e^{-\lambda_1 (l_n - x)}$. Retaining only the larger terms among the above mentioned exponentials, we have

$$j_n(x,t) = \frac{I(t)}{a_n F l_n}\left[\beta_n\sigma_{1n}e^{\lambda_1 x} + \beta_n\kappa_{2n}e^{\lambda_1 (l_n - x)}\right] \quad [A19]$$

Depending on the relative magnitude of the electronic and ionic conductivities, we can write the below for two possibilities:

1. If $\sigma_{1n} >> \kappa_{2n}$, Eq. A19 can be re-written as:

$$j_n(x,t) \approx \frac{I(t)}{a_n F l_n}\left[e^{\log(\beta_n\sigma_{1n})}e^{\lambda_1 x}\right] \quad [A20]$$

or

$$j_n(x,t) \approx \frac{I(t)}{a_n F l_n}\exp\left[d_{n1}(t)\left(\frac{x}{l_n} - \frac{1}{d_{n2}(t)}\right)\right] \quad [A21]$$

where

$$d_{n1} = \lambda_1 l_n \text{ and } d_{n2} = -\lambda_1 l_n / \log(\beta_n\sigma_{1n})$$

2. If $\sigma_{1n} << \kappa_{2n}$

$$j_n(x,t) \approx \frac{I(t)}{a_n F l_n}\left[e^{\log(\beta_n\kappa_{2n})}e^{\lambda_1 (l_n - x)}\right] \quad [A22]$$

The above can be rewritten as

$$j_n(x,t) \approx \frac{I(t)}{a_n F l_n}\exp\left[d_{n1}(t)\left(\frac{l_n - x}{l_n} - \frac{1}{d_{n2}(t)}\right)\right] \quad [A23]$$

where

$$d_{n1} = \lambda_1 l_n \text{ and } d_{n2} = -\lambda_1 l_n / \log(\beta_n\kappa_{2n})$$

One can find similar exponential forms for the positive electrode, as given below for the two possibilities:

1. If $\sigma_{1p} >> \kappa_{2p}$

$$j_p(x,t) = -\frac{I(t)}{a_p F l_p}\exp\left[d_{p1}(t)\left(\frac{(l_n + l_s + l_p) - x}{l_p} - \frac{1}{d_{p2}(t)}\right)\right] \quad [A24]$$

2. If $\sigma_{1p} << \kappa_{2p}$

$$j_p(x,t) = -\frac{I(t)}{a_p F l_p}\exp\left[d_{p1}(t)\left(\frac{x - (l_n + l_s)}{l_p} - \frac{1}{d_{p2}(t)}\right)\right] \quad [A25]$$

List of Symbols

a	Specific surface area of active materials, $m^2\ m^{-3}$
c_1	Solid phase concentration in active material spheres, mol m^{-3}
c_2	Electrolyte concentration, mol m^{-3}
c_s	Solid phase concentration at the surface of active material spheres, mol m^{-3}
d	Reaction profile parameters
D_1	Solid diffusivity in active material spheres, $m^2\ s^{-1}$
D_2	Effective electrolyte diffusivity in the porous domains, $m^2\ s^{-1}$
F	Faraday's constant, 96487 C mol^{-1}
I	External current density, A m^{-2}
j	Reaction rate, mol $s^{-1}\ m^{-2}$
J	Volumetric current density, A m^{-3}
k_k	Surface reaction rate constant in $k = n, p$ electrodes, (mol $s^{-1}\ m^{-2}$) (mol m^{-3})$^{-1.5}$
l	Thickness of domain, m
L	Total cell thickness in through-plane direction, m
n_m	Coefficients of electrolyte concentration profile in anode ($m = 0, \cdots 3$)
p_m	Coefficients of electrolyte concentration profile in cathode ($m = 0, \cdots 3$)
R_k	Radius of the active material spheres in $k = n, p$ electrodes, m
R	Universal gas constant, 8.314 J $mol^{-1}\ K^{-1}$
r	Radial coordinate, m
S	Species source term, mol $m^{-3}\ s^{-1}$
s_m	Coefficients of electrolyte concentration profile in separator ($m = 0, \cdots 2$)
SOC	state of charge = c_{sk}/c_{skmax}
T	Temperature, K
t	Time, s
t_+	Transference number of the electrolyte
U	Open circuit potential of electrode, V
V	Voltage, V
x	Through plane coordinate, m

Greek

α	Transfer coefficient
ε	Porosity
η	Overpotential
κ	Ionic conductivity (Sm^{-1})
σ	Electronic conductivity (Sm^{-1})
Φ_1	Solid phase potential (V)
Φ_2	Electrolyte phase potential (V)

Subscripts

0	Initial condition, exchange, parameter index for electrolyte concentration profiles
1	Electrode phase, parameter index for reaction rate and electrolyte concentration profiles
2	Electrolyte phase, parameter index for reaction rate and electrolyte concentration profiles
3	Parameter index for electrolyte concentration profiles
cell	Cell
exp	Experimental
in	Separator interface of the negative electrode
ip	Separator interface of the positive electrode
k	Domain (anode, separator or cathode)
mid	Middle
mod	Model
max	Maximum
n	Anode
p	Cathode
r	Radial gradient
s	Separator

Operators

$\langle .. \rangle$	Volume average in a domain (anode, separator or cathode)
$\tilde{..}$	Volume average within an active material sphere in electrodes

ORCID

Ashwini Kumar Sharma https://orcid.org/0000-0003-0329-3542
Krishnan S. Hariharan https://orcid.org/0000-0002-1533-9897

References

1. A. Opitz, P. Badami, L. Shen, K. Vignarooban, and A. M. Kannan, *Renewable and Sustainable Energy Reviews*, **68**, 685 (2017).
2. S. Hardman, A. Chandan, G. Tal, and T. Turrentine, *Renewable and Sustainable Energy Reviews*, **80**, 1100 (2017).
3. C. D. Rahn and C. Y. Wang, *Battery Systems Engineering*, p. 193, John Wiley & Sons, Ltd., (2013).
4. G. L. Plett, *Battery Management Systems – Volume 1, Battery Modeling*, Chapter 2, Artech House, Boston (2015).
5. M. Doyle, T. F. Fuller, and J. Newman, *J. Electrochem. Soc.*, **140**, 1526 (1993).
6. T. F. Fuller, M. Doyle, and J. Newman, *J. Electrochem. Soc.*, **141**, 1 (1994).
7. T. F. Fuller, M. Doyle, and J. Newman, *J. Electrochem. Soc.*, **141**, 982 (1994).
8. C. R. Pals and J. Newman, *J. Electrochem. Soc.*, **142**, 3274 (1995).
9. C. R. Pals and J. Newman, *J. Electrochem. Soc.*, **142**, 3282 (1995).
10. W. B. Gu and C. Y. Wang, *J. Electrochem. Soc.*, **147** 2910 (2000).
11. V. Srinivasan and C. Y. Wang, *J. Electrochem. Soc.*, **150**, A98 (2003).
12. K. Smith and C. Y. Wang, *J. Electrochem. Soc.*, **160**, 662 (2006).
13. Y. Ji, Y. Zhang, and C. Y. Wang, *J. Electrochem. Soc.*, **160**, A636 (2013).
14. S. Basu, R. S. Patil, S. Ramachandran, K. S. Hariharan, S. M. Kolake, D. Oh T.Song, T. Yeo, and S. Doo, *J. Power Sources*, **283**, 132 (2015).
15. P. Ramadass, B. Haran, P. M. Gomadam, R. White, and B. N. Popov, *J. Electrochem. Soc.*, **151**, A196 (2004).
16. G. Ning, R. E. White, and B. N. Popov, *Electrochim. Acta*, **51**, 2012 (2006).
17. M. T. Lawder, P. C. Northrop, and V. R. Subramanian, *J. Electrochem. Soc.*, **161**, A2099 (2014).
18. T. Tanim and C. D. Rahn, *J. Power Sources*, **294**, 239 (2015).
19. V. Srinivasan and J. Newman, *J. Electrochem. Soc.*, **151**, A1530 (2004).
20. V. Remadesigan, P. W. C. Northrop, S. De, S. Santhagopalan, R. D. Braatz, and V. R. Subramanian, *J. Electrochem. Soc.*, **159**, R31 (2012).
21. P. W. C. Northrop, B. Suthar, V. Ramadesigan, S. Shanthanagopalan, R. D. Braatz, and V. R. Subramanian, *J. Electrochem. Soc.*, **161**, E3149 (2014).
22. P. W. C. Northrop, M. Pathak, D. Rife, S. De, S. Shanthanagopalan, and V. R. Subramanian, *J. Electrochem. Soc.*, **162**, A940 (2015).
23. S. Wang, M. Verbrugge, J. S. Wang, and P. Liu, *J. Power Sources*, **214**, 399 (2012).
24. A. V. Randall, R. D. Perkins, X. Zhang, and G. L. Plett, *J. Power Sources*, **209**, 282 (2012).
25. G. Ning and B. N. Popov, *J. Electrochem. Soc.*, **151**, A1584 (2004).
26. C. Speltino, D. Di Domenico, G. Fiengo, and A. Stefanopoulou, *Joint 48th IEEE Conf. Decision Cont. and 28th Chinese Cont. Conf.*, Shanghai, P.R. China, 3276 (2009).
27. V. R. Subramanian, V. Boovaragavan, and V. D. Diwakar, *Electrochem. Solid-State Lett.*, **10**, A255 (2007).
28. K. A. Smith, C. D. Rahn, and C. Y. Wang, *Energy Conv. Mgmt.*, **48**, 2565 (2007).
29. V. R. Subramanian, V. Boovaragavan, V. Ramadesigan, and M. Arabandi, *J. Electrochem. Soc.*, **156**, A260 (2009).
30. M. Guo, G. Sikha, and R. E. White, *J. Electrochem. Soc.*, **158**, A122 (2011).
31. P. W. C. Northrop, V. Ramadesigan, S. De, and V. R. Subramanian, *J. Electrochem. Soc.*, **158**, A1461 (2011).
32. V. Senthil Kumar, *J. Power Sources*, **222**, 426 (2013).
33. P. Gambhire, N. Ganesan, S. Basu, K. S. Hariharan, S. M. Kolake, T. Song, D. Oh, T. yeo, and S. Doo, *J. Power Sources*, **290**, 87 (2015).
34. S. K. Rahimian, S. Rayman, and R. E. White, *J. Power Sources*, **224**, 180 (2013).
35. W. Luo, C. Lyu, L. Wang, and L. Zhang, *J. Power Sources*, **241**, 295 (2013).
36. A. Jokar, B. Rajabloo, M. Desilets, and M. Lacroix, *J. Electrochem. Soc.*, **163**, A2876 (2016).
37. B. Rajabloo, A. Jokar, M. Desilets, and M. Lacroix, *J. Electrochem. Soc.*, **164**, A99 (2017).
38. H. E. Perez, S. Dey, X. Hu, and S. J. Moura, *J. Electrochem. Soc.*, **164**, A1679 (2017).
39. C. Lin, A. Tang, and J. Xing, *Applied Energy*, **207**, 394 (2017).
40. C. Lin, A. Tang, and J. Xing, *Applied Energy*, **207**, 394 (2017).
41. M. Pathak, S. Kolluri, and V. R. Subramanian, *J. Electrochem. Soc.*, **164**, A973 (2017).
42. J. L. Lee, A. Chemistruck, and G. L. Plett, *J. Power Sources*, **220**, 430 (2012).
43. J. L. Lee, L. L. Aldrich, K. D. Stetzel, and G. L. Plett, *J. Power Sources*, **255**, 85 (2014).
44. A. Rodriguez and G. L. Plett, *J. Energy Storage*, **11**, 219 (2017).
45. Y. Ye, S. Yixiang, N. Cai, and X. He, *J. Power Sources*, **199**, 227 (2012).
46. V. R. Subramanian, V. D. Diwakar, and D. Tapriyal, *J. Electrochem. Soc.*, **152**, A2002 (2005).
47. V. Ramadesigan, V. Boovaragavan, J. C. Pirkle Jr., and V. R. Subramanian, *J. Electrochem. Soc.*, **157**, A854 (2010).
48. P. C. Urisanga, D. Rife, S. De, and V. R. Subramanian, *J. Electrochem. Soc.*, **162**, A852 (2015).
49. M. Guo and R. E.White, *J. Power Sources*, **198**, 322 (2012).
50. L. Cai and R. E. White, *J. Electrochem. Soc.*, **156**, A154 (2009).
51. K. A. Smith, CC. D Rahn, and C.-Y. Wang, *J. Dyn. Sys., Meas., Control*, **130**, 011012 (2008).
52. K. Smith and C.-Y. Wang, *J. Power Sources*, **161**, 628 (2006).
53. S. Liu, *Solid State Ionics*, **177**, 53 (2006).